

The Conjugate Field Fidelity
Susceptibility (CFFS): A Novel
Computational Approach to Quantum
Phase Transitions

By
MICHAEL THESBERG, B.SC.

*A Thesis
Submitted to the School of Graduate Studies
in Partial Fulfilment of the Requirements
for the Degree
Master of Science*

*McMaster University
©by Michael Thesberg, August 2010*

MASTER OF SCIENCE (2010)
(Physics and Astronomy)

McMaster University
Hamilton, Ontario

TITLE: The Conjugate Field Fidelity Susceptibility (CFFS): A
Novel Computational Approach to Quantum Phase Transitions

AUTHOR: Michael Thesberg, B.Sc. (McMaster University)

SUPERVISOR: Professor Erik S. Sørensen

NUMBER OF PAGES: vii, 212

Abstract

This work introduces a new technique for the determination of quantum phase transitions known as the Conjugate Field Fidelity Susceptibility (CFFS) approach. The CFFS method draws highly on the Quantum Information concept of quantum fidelity susceptibility. An initial introduction to the computational tricks needed to feasibly calculate quantum fidelities will be given. Following this will be a discussion of the nature, derivation and applications of the quantum fidelity and fidelity susceptibilities. Then the CFFS technique will be described before applying it to identify a BKT (Berezinsky-Kosterlitz-Thouless) transition in the Next-Nearest Neighbour Heisenberg Spin Chain. Finally, the method will be applied to confirm the more robust phase diagram of the Next-Nearest Neighbour Heisenberg model on an anisotropic triangular lattice.

Acknowledgements

I would like to thank Erik S. Sørensen for his aid and guidance, as well as SharcNET for access to their computing resources and the McMaster Physics and Astronomy department for its support. I would also like to thank the many people who provided me with feedback on this thesis.

Contents

1	Introduction, Frustrated Systems and Exact Diagonalization	1
2	The Lanczos Method	2
2.1	The Need to Reduce the Hilbert Space	3
2.2	Rewriting the Hamiltonian	4
2.3	Symmetries	5
2.3.1	Spin Inversion Symmetry	5
2.3.2	SU(2) Symmetry (Total S^z Conservation)	6
2.3.3	Translational Symmetry	7
2.3.4	Symmetries; A Conclusion	8
2.4	The Final Trick: Parallelization	8
2.5	The Tally	9
3	Quantum Fidelity and Quantum Phase Transitions	10
3.1	Definition of the Quantum Fidelity	10
3.1.1	The Transverse Field Ising Model: An Example	10
3.1.2	Quantum Fidelity and Quantum Phase Transitions: A General Discussion	12
3.1.3	A Brief History	13
3.2	Fidelity Susceptibility	13
3.2.1	Fidelity Susceptibility and the Derivatives of the Ground State Energy	14
3.2.2	Fidelity Susceptibility and Dynamic Structure Factors; A Connection	16
3.2.3	The Fidelity Susceptibility and Higher-Order Transitions	16
4	The Heisenberg Next-Nearest Neighbour Spin Chain	17
4.1	The Conjugate Field Fidelity and Fidelity Susceptibility	18
4.2	The Dimerized Susceptibility	19
4.3	Method and Results	20
4.3.1	Scaling of the Fidelity Susceptibility	21
4.3.2	Results (cont.)	21
4.4	Discussion	22
5	The Anisotropic Triangular Model	23
5.1	An Introduction; Cs_2CuCl_4	23
5.2	The Proposed Phase Diagram $J_2 = 0$	24
5.3	The Proposed Phase Diagram $J_2 \neq 0$	24
5.4	The Susceptibilities	25
5.4.1	The Dimerized Susceptibility	25
5.4.2	The Collinear-Antiferromagnetic (CAF) Susceptibility	25
5.4.3	The Spiral Susceptibility	26
5.5	The Method	27
5.6	The Results	28
5.7	Discussion	30
6	Conclusion and Summary	32
7	Future Work	32
8	Bibliography	32

List of Figures

1	Fidelity of the Transverse Field Ising Model	12
2	Diagram of the Dimerized Susceptibility in One-Dimension	19
3	Sample Graph of χ_D vs. J_2	20
4	Sample Intersection of χ_D/L^3 vs. J_2	21
5	Scaling of χ_D	22
6	Power-Law Fitting of χ_D/L^3 Intersection Points as a Function of L	22
7	Diagram of the Anisotropic Triangular Lattice	23
8	The Phase Diagram of the Heisenberg Anisotropic Triangular Model as Suggested by the Literature	24
9	Diagram of Dimerized Susceptibility	26
10	Diagram of Collinear-Antiferromagnetic Susceptibility	26
11	Diagram of Spiral Susceptibility	27
12	Vertical Cross-Section of the HATM Phase Diagram	28
13	Ordinary Fidelity Susceptibility at Constant J_2	29
14	Horizontal Cross-Section of the HATM Phase Diagram	29
15	Results from the Application of the Intersecting χ_D/L^3 Curves Method to the HATM	30
16	Additional Horizontal Cross-Sections	31
17	New Phase Diagram	31

1 Introduction, Frustrated Systems and Exact Diagonalization

Since the discovery of high temperature superconductors (i.e. unconventional superconductors) in the late 1980's the theory and study of quantum phase transition has gathered an enormous amount of interest. Of particular interest are quantum systems that are confined in dimensionality (i.e. one-dimensional and two-dimensional systems), as these systems are believed to be crucial in unconventional superconduction. However, despite concerted efforts, the determination of quantum transitions in general is still a very difficult task. A general methodology for identifying all possible transitions simply does not exist and thus an ad hoc series of techniques must be applied, each technique only having limited effectiveness at identifying certain specific classes of transitions. None of these techniques have been shown to identify all transitions. Especially difficult are transitions of infinite order or those topological in nature. These transitions, which are not accompanied by a divergence of either the first or second derivative of the ground-state energy, repeatedly resist any form of standardized probe.

It is the purpose of this work to, *at the very least*, provide a new tool for the proverbial quantum phase transition toolbox. However, the method described herein also shows some promise as a means of pinpointing many types of transitions that are notoriously elusive and which have previously resisted identification by other methods.

Our approach draws its inspiration from the quantum information notions of quantum fidelity and fidelity susceptibility and expands upon these ideas to yield a new perspective on quantum phase transitions. Here we will demonstrate our method's ability to not only qualitatively but quantitatively identify a Berezinsky-Kosterlitz-Thouless-type (BKT)[1, 2] transition in the one-dimensional $J - J'$ Heisenberg Spin Chain and to qualitatively confirm the existence of certain transitions in the Next-Nearest-Neighbour Heisenberg Anisotropic Triangular system.

For reference the Next-Nearest-Neighbour Heisenberg Hamiltonian is

$$H = J_1 \sum_{\langle i,j \rangle} \vec{S}_i \cdot \vec{S}_j + J_2 \sum_{NNN} \vec{S}_i \cdot \vec{S}_j \quad (1.1)$$

where the J_1 sum over $\langle i, j \rangle$ represents a sum over nearest neighbours and the J_2 sum is over all next-nearest neighbours (J 's > 1 represent antiferromagnetic interactions). It can more compactly be written as

$$H = \sum_{\langle i,j \rangle} J_{ij} \vec{S}_i \cdot \vec{S}_j \quad (1.2)$$

where it is understood that the sum $\langle i, j \rangle$ is now over both nearest neighbours *and* next-nearest neighbours and the value of J_{ij} is either J_1 or J_2 accordingly. With exception of a small perturbative external field described later, the Heisenberg Hamiltonian will be the sole Hamiltonian explored herein. We will begin with a discussion of the numerical considerations and computational techniques employed in our new method, followed by a general introduction to the quantum fidelity as well as the fidelity susceptibility for those uninitiated. Finally, the specifics of our new Conjugate Field Fidelity Susceptibility (CFFS) approach will be described and its application to the spin-1/2 chain and two-dimensional anisotropic triangular lattice will be detailed.

2 The Lanczos Method

The numerical crux of this work lies in determining the ground-state energies and eigenvectors of a given Hamiltonian. The naive approach to such a problem would be to generate a matrix representation of the Hamiltonian and fully diagonalize it to find all its eigenvectors and eigenvalues. However, even if the energy spectrum of a system wasn't infinite (which they will be) this is completely infeasible on a computational level. To this end the Lanczos method is employed. The Lanczos (pronounced LAWN-T-sosh) method is a modified power series method. One starts with a random trial guess at the system's ground-state eigenvector, then applies the method iteratively, eventually converging (one hopes) to the eigenvector corresponding to the smallest eigenvalue. This is the ground-state eigenvector and the smallest eigenvalue is the ground-state energy. The method not only determines the ground-state eigenvector but can also reliably generate the eigenvectors of the first few lowest lying states. It cannot, however, be used to find any but the lowest lying states. In general, for complicated numerical reasons, the larger the energy gap between the ground-state and the first excited state the more accurate the first excited state's eigenvector will be.

The Lanczos method consists of a number of distinct steps. First the following Lanczos algorithm is allowed to iterate, the more iterations the more accurate:

Lanczos Algorithm

```
v(1)= random_normalized_vector
v(0)=0
beta(0)=0
for j=1 to m
  w(j) = matrix_multiplication(H,v(j)) - beta(j)*v(j-1)
  alpha(j) = inner_product(w(j),v(j))
  w(j) = w(j) - alpha(j)*v(j)
  beta(j+1) = absolute_value(w(j))
  v(j+1) = w(j) / beta(j+1)
end
```

It should be noted here that there are many minor variations on the basic Lanczos algorithm. The algorithm above is due to early pioneering work by C. C. Paige[3][4] on the Lanczos method and has been determined to be the most numerically stable. At the termination of the m loops of this algorithm one then uses the calculated $\alpha(1) \dots \alpha(m)$ and $\beta(1) \dots \beta(m)$ to form a tridiagonal matrix called the Lanczos matrix:

$$T_{mm} = \begin{pmatrix} \alpha_1 & \beta_2 & & & & 0 \\ \beta_2 & \alpha_2 & \beta_3 & & & \\ & \beta_3 & \alpha_3 & \ddots & & \\ & & \ddots & \ddots & & \\ & & & \beta_{m-1} & & \\ 0 & & & \beta_{m-1} & \alpha_{m-1} & \beta_m \\ & & & & \beta_m & \alpha_m \end{pmatrix} \quad (2.1)$$

The eigenvalues of this Lanczos matrix are the numerical estimates of the m lowest eigenvalues of the Hamiltonian with the lowest eigenvalue (i.e. the ground-state) being the most accurate and the m th lowest eigenvalue being the least accurate. The corresponding eigenvectors are then generated by

$$y_i = V_m u_i^{(m)} \quad (2.2)$$

where y_i is the i th eigenvector, V_m is the matrix whose column vectors are $v(1) \dots v(m)$ and $u_i^{(m)}$ is the eigenvector corresponding to the i th lowest eigenvalue of the Lanczos matrix T_{mm} . The calculation is complete when the eigenvalues and eigenvectors have been calculated to sufficient accuracy. In essence the Lanczos method takes an $n \times n$ matrix, which is usually sparse, and reduces it, after m steps, to an $m \times m$ tridiagonal matrix whose eigenvalues represent the lowest eigenvalues of the much larger $n \times n$ system. This $m \times m$ matrix (since, $m \ll n$) can easily be solved via a more conventional method, such as the Jacobian method used in this work, to determine the low lying energy eigenvalues of the system, as well as the corresponding eigenvectors.

There are many obvious advantages to the Lanczos method. For one, it iteratively converges most quickly to the *lowest* eigenvalue/eigenvectors and therefore, one need not even attempt to solve for the whole energy spectrum of the Hamiltonian. When studying quantum phase transitions, these low lying states are by far the most important.[5] For another, the fundamental algorithm can be rewritten such that one only has to save/store two eigenvectors and the Hamiltonian matrix[6]; the extreme utility of this fact will become obvious later and is a huge improvement from the m eigenvectors one need store when applying the basic algorithm. There are also many subtle advantages of the Lanczos approach over similar power methods, such as the Schurm or Naive Power Method. For a more comprehensive discussion see "Lanczos Algorithms for Large Symmetric Eigenvalue Computations" by Cullum and Willoughby[7]. However, despite the many advantages of the Lanczos algorithm over a more naive approach, all but the smallest systems are still computationally intractable to the Lanczos method alone.

2.1 The Need to Reduce the Hilbert Space

To see why the Lanczos approach alone is insufficient let's consider a spin-1/2 system. If we have, say, a 2 site system then the eigenbasis of our Hamiltonian contains the following 4 elements (in the z-basis):

$$|\uparrow\uparrow\rangle, |\uparrow\downarrow\rangle, |\downarrow\uparrow\rangle, |\downarrow\downarrow\rangle. \quad (2.3)$$

If we have a three-site system our eigenbasis is:

$$|\uparrow\uparrow\uparrow\rangle, |\uparrow\uparrow\downarrow\rangle, |\uparrow\downarrow\uparrow\rangle, |\uparrow\downarrow\downarrow\rangle, |\downarrow\uparrow\uparrow\rangle, |\downarrow\uparrow\downarrow\rangle, |\downarrow\downarrow\uparrow\rangle, |\downarrow\downarrow\downarrow\rangle, \quad (2.4)$$

and so on. In general, for a system of size N there will be 2^N possible permutations that form the spin-1/2 eigenbasis. Thus, the eigenvectors of a system of size N will have 2^N elements and a matrix representation of the Hamiltonian will have $(2^N)^2 = 2^{2N}$ components.

If we now consider a modern computer, it might have 4 GB of RAM. That's $4 \times 2^{30} = 4\,294\,967\,296$ bytes. If we assume that we wish to calculate our eigenvalues to double precision (approximately 15 digits accuracy) then each numerical value, be it an element of the eigenvector or component of the matrix, will take up 8 bytes (32 bits) of space. Even if we make the unrealistic assumption that there is absolutely nothing else in our computer's RAM then the largest system that could be solved using the Lanczos method (which requires 2 eigenvectors and the Hamiltonian matrix) is

$$(2 \times 2^N + 2^{2N}) \text{ values} \cdot \left(8 \frac{\text{bytes}}{\text{value}}\right) = (2^{N+4} + 2^{2N+3}) \text{ bytes} = 4\,294\,967\,296 \text{ bytes}$$

$$N \sim 14.$$

A maximum system size of 14 is far too small to be useful. Fortunately, all is not lost. There are a few tricks that can be applied to salvage the situation. Firstly, the Hamiltonian

of a Heisenberg system in particular (which are the systems being studied here) can be rewritten in a clever way that removes the need to save the Hamiltonian matrix to memory at all; secondly, the size of the Hilbert space can be greatly reduced by considering specific symmetries of the system; and finally the amount of memory space available can be increased through the use of parallel computing. We will now look at these three techniques in more detail.

2.2 Rewriting the Hamiltonian

By far the largest portion of the total memory space required when performing Lanczos exact diagonalization is consumed by storing the Hamiltonian matrix. It requires 2^{2N} doubles to be saved to memory. This is huge compared to the much smaller 2×2^N doubles required for the two eigenvectors. If one could avoid storing the Hamiltonian matrix it would go a long way towards simulating useful system sizes. Fortunately, in the case of the Heisenberg Model, there is a way to do just that.

First we consider the Heisenberg Hamiltonian (we neglect the second-nearest-neighbour term but it follows identically)

$$H = J \sum_{\langle i,j \rangle} (\vec{S}_i \cdot \vec{S}_j) \quad (2.5)$$

and, for ease of exposition, we consider a two state system whose eigenbasis is then

$$|\uparrow\uparrow\rangle, |\uparrow\downarrow\rangle, |\downarrow\uparrow\rangle, |\downarrow\downarrow\rangle. \quad (2.6)$$

The matrix representation of a single interaction term in this Hamiltonian is then

$$\vec{S}_i \cdot \vec{S}_j = \frac{1}{4} \begin{pmatrix} 1 & 0 & 0 & 0 \\ 0 & -1 & 2 & 0 \\ 0 & 2 & -1 & 0 \\ 0 & 0 & 0 & 1 \end{pmatrix}. \quad (2.7)$$

Now the clever part lies in realizing that this looks very similar to the pivot matrix

$$P_{ij} = 2\vec{S}_i \cdot \vec{S}_j + \frac{1}{2}I = \begin{pmatrix} 1 & 0 & 0 & 0 \\ 0 & 0 & 1 & 0 \\ 0 & 1 & 0 & 0 \\ 0 & 0 & 0 & 1 \end{pmatrix}. \quad (2.8)$$

and in fact, it can be shown that the Heisenberg Hamiltonian for a system of any size can be rewritten as

$$H = J \sum_{\langle i,j \rangle} (\vec{S}_i \cdot \vec{S}_j) = \frac{J}{2} \left(\sum_{\langle i,j \rangle} P_{ij} - \frac{L}{2}I \right) \quad (2.9)$$

where L is the total number of bonds. The reason this restating of the Hamiltonian is so useful is because the pivot matrix P_{ij} acts to interchange two components of the vector that the Hamiltonian acts on. For example:

$$P_{12} \begin{pmatrix} x_0 \\ x_1 \\ x_2 \\ x_3 \\ \vdots \\ x_n \end{pmatrix} = \begin{pmatrix} x_0 \\ x_2 \\ x_1 \\ x_3 \\ \vdots \\ x_n \end{pmatrix}. \quad (2.10)$$

Thus the Hamiltonian is reduced to a specific sequence of row interchanges (and addition of a constant). Therefore, one can hard-code this sequence of component swaps and not bother to save the $2^N \times 2^N$ Hamiltonian matrix at all. In other words, one can create a function in one's program called `HAMILTONIAN` that can act on a vector whose end result is to swap the various components of the vector in the way the Hamiltonian would. For example, one might consider the eigenket $\alpha | \uparrow \downarrow \downarrow \uparrow \rangle$; the action of a matrix multiplication of a single term of the sum in the Hamiltonian, say the $S_1 \cdot S_3$ might simply produce the state $\alpha | \uparrow \downarrow \uparrow \rangle$. Therefore, why perform the matrix multiplication at all (and thus bother to save the matrix) when instead one could have a function which swaps the 1st and 3rd spins in the system. The end result is the same but this way one need not perform a huge matrix multiplication of the form $Hx_0 = x_1$ or save the matrix H to memory. Although this trick frees up a great amount of space there is still more that can be done to increase the maximum computable system size. Let us now look at system symmetries.

2.3 Symmetries

The complete Hilbert space of a spin-1/2 system has 2^N elements. However, for every symmetry of the Hamiltonian there are many states that are actually identical. Therefore, when storing our eigenvectors we need not save all 2^N entries, but only those which are distinct. To be more concrete let's focus our discussion on the Heisenberg Hamiltonian and for simplicity, we will consider a four site system (though everything discussed can easily be generalized). The complete eigenbasis of this system has $2^4 = 16$ elements which are:

$$|0000\rangle, |0001\rangle, |0010\rangle, |0011\rangle, |0100\rangle \dots |1111\rangle \quad (2.11)$$

where we use 0 to represent \downarrow and 1 to represent \uparrow . By exchanging the arrow symbols for numbers it is easy to see how one can give a unique index to each state. $|0000\rangle$ is state 0, $|1010\rangle$ is state 10 and so on. As we reduce the Hilbert space, the task of assigning a unique index to each state becomes a great deal more difficult, sometimes prohibitively so.

2.3.1 Spin Inversion Symmetry

The Heisenberg Hamiltonian is invariant under the spin inversion operator. In other words, if we invert every spin in the system the Hamiltonian

$$H = J \sum_{\langle i,j \rangle} ((-\vec{S})_i \cdot (-\vec{S})_j) = J \sum_{\langle i,j \rangle} ((-1)^2 \vec{S}_i \cdot \vec{S}_j) = J \sum_{\langle i,j \rangle} (\vec{S}_i \cdot \vec{S}_j) \quad (2.12)$$

remains unchanged. Therefore, the physics related to the states $|1001\rangle$ and $|0110\rangle$ are identical. This is of great use in terms of storage because, when considering the ground-state of a system, we can assume these symmetric pairs form a singlet/triplet of the form

$$\frac{|0110\rangle \pm |1001\rangle}{\sqrt{2}} \quad (2.13)$$

where the \pm is determined by the parity of the system. In general determining the parity can be a little bit tricky as it depends on the size of the system, the type of Hamiltonian, as well as the total S . To find it one can simply draw out a few small systems for a given Hamiltonian and a relatively simple pattern of even and odd parity as a function of system size should emerge (for example, for even sized systems in $S = 0$ the parity is negative, in odd sized it is positive).

By symmetrizing ones' states one need only track and store *one* of the two states since the other will have identical coefficients. It is convention to keep the state represented by the lowest valued binary number and discard the other (so in our example $|0110\rangle$ is kept and $|1001\rangle$ discarded when storing our eigenvector). Thus, the new symmetrized eigenbasis for our four-site system (as well as accompanying indices) is

$$0.|0000\rangle, 1.|0001\rangle, 2.|0010\rangle, 3.|0011\rangle, 4.|0100\rangle, 5.|0101\rangle, 6.|0110\rangle, 7.|0111\rangle \quad (2.14)$$

where, for example, the state $|1000\rangle$ is not included since it is really a spin-inversion of the state $|0111\rangle$ which has already been accounted for. Indexing the new spin-inversion symmetric states is thankfully very easy. There are simply half as many states and their label is still their value in binary representation. Unfortunately, none of the other symmetries we will discuss here produce states that can be so easily relabelled. As a final word of warning, one must always remember, when considering this new eigenbasis, that the "state" $|0111\rangle$ no longer simply represents that actual eigenket but instead represents the symmetrized state

$$\frac{|0111\rangle \pm |1000\rangle}{\sqrt{2}}. \quad (2.15)$$

Also a very common Hamiltonian encountered is one with an external field h_z . Such a field breaks spin-inversion symmetry and therefore, with such a Hamiltonian spin-inversion cannot be used to reduce the Hilbert space.

2.3.2 SU(2) Symmetry (Total S^z Conservation)

Another important symmetry of the Heisenberg Hamiltonian is *total S^z conservation*. If one expands out the Hamiltonian

$$\sum_{\langle i,j \rangle} J_{ij} \vec{S}_i \cdot \vec{S}_j = \sum_{\langle i,j \rangle} J_{ij} S_i^x \cdot S_j^x + \sum_{\langle i,j \rangle} J_{ij} S_i^y \cdot S_j^y + \sum_{\langle i,j \rangle} J_{ij} S_i^z \cdot S_j^z \quad (2.16)$$

into a more transparent form by substituting the ladder operators $S_+ = S_x + iS_y$ and $S_- = S_x - iS_y$ one obtains the Hamiltonian

$$\sum_{\langle i,j \rangle} J_{ij} \vec{S}_i \cdot \vec{S}_j = \sum_{\langle i,j \rangle} J_{ij} \frac{1}{2} (S_i^+ \cdot S_j^- + S_i^- \cdot S_j^+) + \sum_{\langle i,j \rangle} J_{ij} S_i^z \cdot S_j^z. \quad (2.17)$$

In this form it is easy to see that the Heisenberg Hamiltonian never raises (lowers) a spin without lowering (raising) one elsewhere. From this we conclude that the total- S_z ($\sum_{i=1}^N S^z$) is conserved.

This is extremely useful since if one knows the total- S_z of the ground-state ($\sum_{i=1}^N S^z = 0$ for systems with even number of sites and 1 (or -1) for those with odd) then one only need consider the region of the Hilbert space with the same total- S_z . In other words, if the ground-state lies within total- $S_z = 0$ then only basis states with even numbers of up and down spins need be considered since the Hamiltonian does not mix states with different total- S_z s. In our example of a four-site system our basis which was reduced to

$$0.|0000\rangle, 1.|0001\rangle, 2.|0010\rangle, 3.|0011\rangle, 4.|0100\rangle, 5.|0101\rangle, 6.|0110\rangle, 7.|0111\rangle \quad (2.18)$$

can be further reduced to

$$1.|0011\rangle, 2.|0101\rangle, 3.|0110\rangle. \quad (2.19)$$

By applying both spin-inversion symmetry and total- S_z a 16 member basis has been reduced to a 3 member basis. This is a huge improvement! In general the exact factor by which the total- S_z symmetry reduces a Hilbert space depends on the Hamiltonian of the system and what value of $\sum_{i=1}^N S^z$ the ground-state lies in. Though, it can roughly be approximated to be of the order of N .

The main drawback of the total- S_z symmetry is that once applied it becomes very difficult to relabel the states. One can see why this is not easy. There is no obvious way of determining the bit-pattern of the third lowest basis state that has exactly as many up spins as down spins and is the lower valued member of a spin-inversion pair. In order to label these states one is forced to compile a look-up table which maps each possible bit-pattern to its index (whether it's the fifth state or the thirteenth). This look-up table must, unfortunately, be saved to memory and thus takes up more space. There are however, elaborate, methods for reducing the memory space required to save one of these look-up tables by constructing them in clever ways. Though, even the most naive approach would produce a look-up table that is *significantly* smaller than 2^N and thus the net result is still a huge savings in space. For a more thorough discussion of the fine points of indexing states see the excellent paper by H.Q. Lin [6]

2.3.3 Translational Symmetry

Translational symmetry is another symmetry which is often invoked for the purpose of reducing a Hilbert space; and by far the most difficult to implement computationally. For this reason it was rarely used in these works. The basic idea, however, is rather simple.

If, with periodic boundary conditions, a system's Hamiltonian is unchanged by a finite translation then the system is said to have *translational symmetry*. For example, the Heisenberg chain Hamiltonian is invariant under a translation of a single site to the right or the left (i.e. it is unchanged if all spins are moved one site to the left or right):

$$H = J_1 \sum_{i=1}^N \vec{S}_{i+1} \cdot \vec{S}_{(i+1)+1} + J_2 \sum_{i=1}^N \vec{S}_{i+1} \cdot \vec{S}_{(i+2)+1} = -J_1 \sum_{i=1}^N \vec{S}_i \cdot \vec{S}_{i+1} - J_2 \sum_{i=1}^N \vec{S}_i \cdot \vec{S}_{i+2} \quad (2.20)$$

Thus the Heisenberg chain has translational symmetry. This can be used to reduce the Hilbert space by representing all states that are translations of each other by a single Bloch state of the form

$$P_k = \frac{1}{M} \sum_{j=1}^M e^{2\pi i j k / M} T^j \quad (2.21)$$

where T^j is the translation operator which translates a given eigenket by one finite translation, k is an integer (for periodic boundaries) related to the Bloch momentum. The period of the translations (M) is the number of consecutive translations that are required in order to return a state to its original form. For example, the state $|0001\rangle$ needs

$$|0001\rangle \xrightarrow{1st} |0010\rangle \xrightarrow{2nd} |0100\rangle \xrightarrow{3rd} |1000\rangle \xrightarrow{4th} |0001\rangle \quad (2.22)$$

four translation before repeating. The state $|0101\rangle$ only needs two:

$$|0101\rangle \xrightarrow{1st} |1010\rangle \xrightarrow{2nd} |0101\rangle. \quad (2.23)$$

Grouping ones states by translational symmetry has the added advantage of allowing one to confine their calculations to specific values of k , i.e. the momentum. However, the indexing of translationally symmetric bases is extremely complicated and it also introduces complications in swapping components, thus no attempt will be made to discuss it here. For a good introduction see Weiße and Fehske's chapter in *Computational Many-Particle Physics*. [8]

However, with translational symmetry our sample four-site system, with its Hilbert space already reduced to

$$1.|0011\rangle, 2.|0101\rangle, 3.|0110\rangle. \quad (2.24)$$

by means of spin-inversion and total- S^z symmetries, could be further reduced to

$$1.|0011\rangle, 2.|0101\rangle. \quad (2.25)$$

This leaves a measly 2 states from an initial 16, a monumental improvement.

2.3.4 Symmetries; A Conclusion

The three symmetries discussed here are by no means the only ones that can be employed to reduce a Hilbert space; they are, however, the most common. Although it is true that any symmetry of the Hamiltonian can be used, most symmetries require enormous amounts of effort to implement and often for very little gain. One can easily go too far with symmetry applications as there are definite cost/benefit considerations for each new symmetry. For example, it is unlikely to be worthwhile to implement a new symmetry that would reduce a Hilbert space by a factor of two if it increases computation time by a factor of 20 and requires a considerable amount of extra coding. Thus, these three symmetries were the only ones considered and, in fact, for the vast majority of this work only the total- S_z symmetry was used. This was due to the extreme difficulty in implementing translational symmetry and the non-applicability of spin-inversion to systems with an external field (such a field will be introduced later).

2.4 The Final Trick: Parallelization

As is now undoubtedly clear, the primary impediment to computing large system sizes is the memory space required to perform an exact diagonalization. Previously it was shown that this restriction can be slightly relaxed through a clever rewriting of the Hamiltonian and through the exploitation of symmetries. However, additional progress can be made through the use of parallelization.

If one distributes the memory load across, say, 128 computers, each with 4 GB of memory then one could foreseeably compute systems that contain roughly 7 ($2^7 = 128$) more sites. These extra sites could easily make the difference between being able and not being able to perform a scaling-relation or finite-size effect analysis.

However, parallelization is notoriously tricky business. One cannot simply take an algorithm written to be run on a single computer and expect it to run identically across multiple. For one, a given computation may require all computers to have a complete copy

of some dataset (perhaps a matrix or a look-up table). Or perhaps a given computer can only continue to a new iteration after having received some information from another node; thus bottlenecking operations at the slowest computer. The former case would be a serious issue if the Lanczos algorithm were to be performed via repeated matrix multiplications. Each computer would need to process (if not store) every element of the matrix for each multiplication. This would require for an enormous amount of data to be transferred between computers and with parallelization the slowest point in computation is always in such inter-computer communications.

Fortunately, by rewriting the Hamiltonian, as we did previously, most of the difficulties associated with matrix multiplication no longer apply. Each computer, now, simply stores a fraction of each eigenvector needed for the Lanczos method. For example, if there are three computers being used to store a 9 element Hilbert space then elements 1-3 are stored on the first computer, 4-6 on the second and 7-9 on the third. The only communication that occurs is when swapping elements of an eigenket produces a new eigenket which is being stored on another computer.

As an example consider a four-site ($2^4 = 16$ element) system split between two computers. The first computer contains the coefficients for the 1st to 8th elements, which are the eigenkets $|0000\rangle$ to $|1000\rangle$. The second computer then has the 9th to 16th elements ($|1001\rangle$ to $|1111\rangle$). Now let's say the eigenket $|0011\rangle$, which is the 4th element of the vector, has the coefficient α . It is stored on the first computer. If a term of the sum in the Hamiltonian leads to a swapping of the 0th and 3rd bits then the new state is $|1010\rangle$, the 11th element of the vector, which is stored on the other machine. The value of α must then be sent over the network to the second computer.

Though, this requires significantly less communication than direct matrix multiplication it still adds up, for large systems, to an enormous amount of data transferring. Managing these sends and receives is not as simple as it may seem and requires a great deal of consideration as to load-balancing and queuing structures. However, if properly implemented the gain in storage space far exceeds the not inconsiderable loss of speed due to communications. Thus, larger systems than before can be computed.

2.5 The Tally

We begun with an initial, dismal, maximum system size of 14. By applying the techniques discussed above we can greatly improve upon this. By re-writing the Hamiltonian we no longer have to save a 2^{2N} matrix and only need store two 2^N eigenvectors. Spin inversion symmetry halves the Hilbert space; total- S^z reduces it by $\sim N$ and translational symmetry further reduces the system size by a factor of $\sim N$. We will conservatively say that we can combine these for only a reduction of size N (translational symmetry is often too difficult to implement). If we now perform the same calculation as earlier we see that the new maximum system size is:

$$\left(2 \times \frac{2^N}{N}\right) \text{ values} \cdot \left(8 \frac{\text{bytes}}{\text{value}}\right) = \left(\frac{2^{N+4}}{N}\right) \text{ bytes} = 4\,294\,967\,296 \text{ bytes}$$

$$N \sim 33.$$

This is a *huge* improvement over 14. However, using parallelization we can roughly compute another site for each time we double the number of computers. Therefore, if we assume that we are using a relatively standard 128 computers then we can compute an additional 7 sites ($128 = 2^7$). Therefore, potentially one could calculate exact diagonalizations of Heisenberg systems as large as 40! This is quite large and more than adequate for most applications. However, it must be noted that although a system size of 40 can now be *stored*,

a number of the techniques discussed increase processing time. Most notably parallelization. Therefore, though it may be feasible from a *storage perspective* to compute with 40 sites such a simulation may take far too long (years potentially). Such large systems will not be attempted in this work (the maximum used is 30).

3 Quantum Fidelity and Quantum Phase Transitions

3.1 Definition of the Quantum Fidelity

On the face of it the quantum fidelity is a very straightforward and intuitive quantity. It is simply the (absolute) overlap (i.e. inner product) of a quantum state with another state, whose Hamiltonian has been slightly perturbed. Thus, if λ represents some variable of a system Hamiltonian and $\delta\lambda$ is a small perturbation of that variable the fidelity is then written as

$$F(\lambda, \delta\lambda) = |\langle\psi(\lambda)|\psi(\lambda + \delta\lambda)\rangle|. \quad (3.1)$$

As a defined quantity, the quantum fidelity traces its roots to the field of Quantum Information.[7-21] In QI (Quantum Information) one often wants to transfer data across large distances by entangling quantum states. Ideally, one wants zero information loss during these transfers. Thus, in QI, the fidelity represents the "faithfulness", much like in audio reproduction, of the final received state to the initial state. Accordingly, a low quantum fidelity represents a great loss of information across an attempted transfer. It's from this QI application that the quantum fidelity gets its name. Since its inception the quantum fidelity has been re-interpreted many times and has found many new applications. Few of these applications relate directly to loss of quantum information. Thus, as a quantity, the quantum fidelity has in many ways outgrown its name, and has found a place in many fields where it is used in ways having little to do with its origin as a measure of information loss. Perhaps the most recent field to find use for the quantum fidelity is Condensed Matter, for it shows great promise as a means of detecting quantum phase transitions.

3.1.1 The Transverse Field Ising Model: An Example

A relatively simple situation where the fidelity can be employed to detect a quantum phase transition is in the Transverse Field Ising Model (TFIM). The TFIM has the Hamiltonian

$$H = - \sum_{j=1}^N (\sigma_j^x \cdot \sigma_{j+1}^x + h\sigma_j^z) \quad (3.2)$$

where, for simplicity, periodic boundary conditions are assumed ($\sigma_{N+1} = \sigma_1$). This Hamiltonian represents an Ising-like system where an external field is applied perpendicular (transversally) to the chain. The strength of the external field is determined by the constant h and thus h is the only parameter that can be varied. This is a simple system for which it is known that at a specific value of h a quantum phase transition occurs. Let's consider things more closely.

When $h = 0$ there is no external field and thus the states with the lowest energy are those for which

$$\sum_{j=1}^N \sigma_j^x \cdot \sigma_{j+1}^x \quad (3.3)$$

is at a maximum. This will occur when all the spins are parallel and directed in the x direction. There is no preference for the positive or negative x thus both are equally likely and the ground state will be of the form

$$|\Psi_{GS}(h=0)\rangle = \frac{1}{\sqrt{2}}(|\rightarrow\rightarrow\rightarrow\dots\rangle + |\leftarrow\leftarrow\leftarrow\dots\rangle). \quad (3.4)$$

When $h=0$ the system has a long-range ferromagnetic ordering. By looking at the action of σ^z on the system's states

$$\sigma^z|\rightarrow\rangle = |\leftarrow\rangle, \quad \sigma^z|\leftarrow\rangle = |\rightarrow\rangle \quad (3.5)$$

we can see that the transverse field acts to mix the $|\rightarrow\rightarrow\rightarrow\dots\rangle$ and $|\leftarrow\leftarrow\leftarrow\dots\rangle$ degenerate ground-states. Therefore, as h increases from 0 the degeneracy becomes broken. However, the ground-state remains qualitatively the same. This qualitative long-range ordering can be made quantitative by considering the correlation function

$$\Phi(r) = \langle\Psi|\sigma_j^x\sigma_{j+r}^x|\Psi\rangle + \langle\Psi|\sigma_j^y|\Psi\rangle\langle\Psi|\sigma_{j+r}^y|\Psi\rangle. \quad (3.6)$$

Thus, when the correlation function is non-zero in the limit $|r| \rightarrow \infty$ the system is said to show long-range order. If the correlation function vanishes as $|r| \rightarrow \infty$ we say it does not.

If we then consider the other extreme limit $h = \infty$, then states whose spins are oriented parallel to the perpendicular field will have the lowest energies and thus the ground-state is

$$|\Psi_{GS}(h=\infty)\rangle = |\uparrow\uparrow\uparrow\dots\rangle. \quad (3.7)$$

Therefore, for some h between $h=0$ and $h=\infty$ the ground-state must undergo a sudden transition from an ordered ground-state (one where the correlation function does not vanish with distance), to a disordered one (one where the correlation function does vanish with distance). We call this value of h the *critical field strength* (h_c). The difficulty then becomes finding the exact value of h_c . In the case of the TFIM the value can be solved exactly and is found to be $h_c = 1$ [24]. However, it can also be identified numerically through the use of the quantum fidelity.

In the case of the TFIM the parameter perturbed is the field strength, h , and thus the fidelity is

$$F_{TFIM}(h, \delta h) = |\langle\Psi_0(h)|\Psi_0(h+\delta h)\rangle| \quad (3.8)$$

where $|\Psi_0(h_0)\rangle$ indicates the ground-state when $h=h_0$ in the Hamiltonian. When $h \ll h_c$ and $h \gg h_c$ the overlap between $|\Psi_0(h)\rangle$ and $|\Psi_0(h+\delta h)\rangle$ will be very nearly 1 since the ground-state differs by only an infinitesimal amount when h is perturbed. However, if one considers the overlap when the perturbation straddles the transition point h_c such that

$$\text{critical fidelity} = |\langle\Psi_0(h_c - \frac{\delta h}{2})|\Psi_0(h_c + \frac{\delta h}{2})\rangle|, \quad (3.9)$$

then the overlap will be significantly smaller (becoming 0 as $\delta h \rightarrow 0$) since the unperturbed ground-state will lie within the ordered phase and be qualitatively similar to

$$|\Psi_{GS}(h=0)\rangle = \frac{1}{\sqrt{2}}(|\rightarrow\rightarrow\rightarrow\dots\rangle + |\leftarrow\leftarrow\leftarrow\dots\rangle) \quad (3.10)$$

where the ground-state of the perturbed Hamiltonian will be

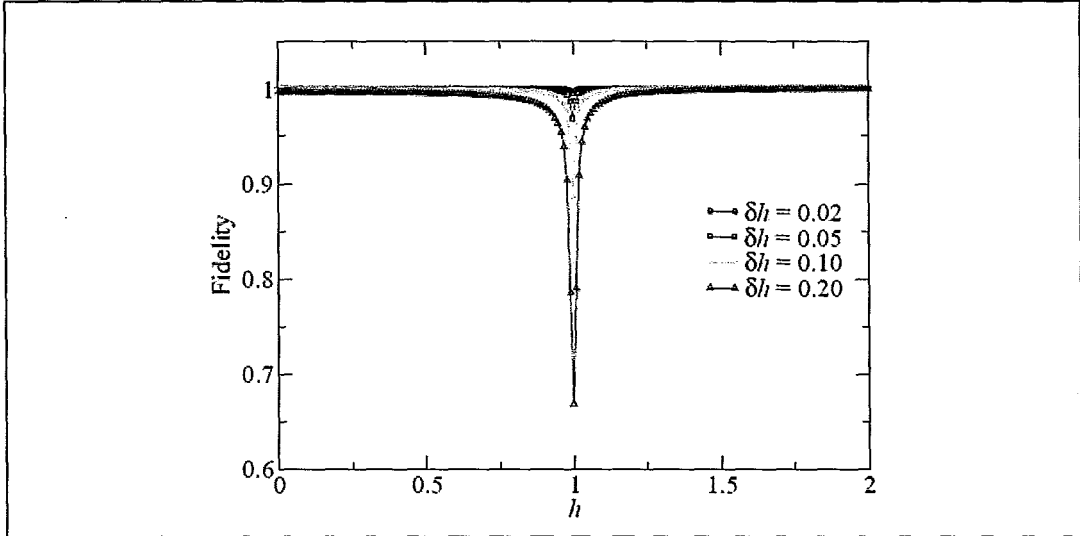


Fig. 1: The fidelity as a function of h in the TFIM. A sharp valley occurs at the critical field strength $h = 1$. This graph was taken from the Topical Review by Gu[24]

$$|\Psi_{GS}(h = \infty) = |\uparrow\uparrow\uparrow \dots\rangle. \quad (3.11)$$

Thus, the inner product of the two will be $\ll 1$ and a graph of the fidelity as a function h will exhibit a sharp dip as can be seen in Fig. 1. By numerically determining the value of h for which the fidelity peaks sharply downwards one can determine h_c to arbitrary accuracy.

3.1.2 Quantum Fidelity and Quantum Phase Transitions: A General Discussion

Since the TFIM has a known analytical solution the fidelity approach may seem pointless. However, the fidelity can easily be applied to many systems that do not have closed form solutions. To be more concrete we must first recognize that any many-body Hamiltonian can be written in the form

$$H(\lambda) = H_0 + \lambda H_1 \quad (3.12)$$

where λ is a parameter that varies and may exhibit a phase transition. This Hamiltonian is completely general and can easily be extended to include multiple parameters. It then becomes

$$H(\lambda_1, \lambda_2, \lambda_3, \dots, \lambda_n) = H_0 + \lambda_1 H_1 + \lambda_2 H_2 + \lambda_1 \lambda_2 H_{12} + \lambda_3 H_3 + \lambda_1 \lambda_3 H_{13} + \dots \quad (3.13)$$

Though, one rarely sees Hamiltonians with coupled terms of the form $\lambda_1 \lambda_2 H_{12}$, but one can include them if necessary. Once the Hamiltonian is understood to be of this form then H_1 can be interpreted as the portion of the Hamiltonian that *drives* a quantum phase transition. Indeed there is a direct relationship between the linear responses of this driving portion of the Hamiltonian and the quantum fidelity. This connection will not be discussed further here but can be found in the seminal article by You *et al.*[25]

In general, any system which undergoes a transition driven by a crossing in energy levels can be detected using the fidelity method. In fact, it need not be a ground-state crossing. For example, in the previously discussed work by Chen *et al.*[26] the transition point of the Next-Nearest Neighbour Heisenberg Chain was calculated by examining a level crossing of the *first excited state* using the fidelity approach.

Quantum phase transitions are often marked by sudden changes in the properties of a system ground-state. Thus, a measure of the change in a ground-state as a system parameter is varied would have great use. Consequently, the appeal of the quantum fidelity as a tool for exploring quantum phase transitions is unmistakable. In addition, since the quantum fidelity is an entirely quantum-informational notion it requires no initial assumptions about order parameters or system symmetries which can often be difficult quantities to infer (if they can be inferred at all). Therefore, any methods based upon the quantum fidelity that could be demonstrated to effectively determine quantum phase transitions would be of tremendous worth.

3.1.3 A Brief History

Before continuing it is worthwhile to briefly discuss the history of the quantum fidelity in Condensed Matter. Perhaps the earliest application of the fidelity towards quantum phase transitions was due to Quan *et al.*[27] who used the Loschmidt Echo, a very similar quantity to the quantum fidelity, to determine the two previously discussed ground-state phases of the Transverse Field Ising Model. Further work by Zanardi and Paunković would then use the true quantum fidelity to identify transitions in the Dicke and the 1D transverse field XY models.[28] Zanardi *et al.* (most notably with Cozzini) would then go on to do much of the early work with the quantum fidelity, applying it to free fermionic systems[29], graphs[30], matrix-product states[31]. Buonsante *et al.* would also apply it to the Bose-Hubbard Model.[32] It was also around this time that the soon to be introduced fidelity susceptibility was developed by You *et al.*[25] These early successes of the quantum fidelity and fidelity susceptibility suggested its promise for identifying transitions outside the typical Landau-Ginzburg-Wilson framework such as those topological in nature of BKT-type.

After these early successes there was a divergence in the studies of the quantum fidelity. The first sub-field focused on the quantum fidelity itself and approached it as a Riemannian tensor quantity. The first works from this perspective are due to Zanardi *et al.*[33], however, significant contributions would then be made by Zhou *et al.* who would explore the relationships between the fidelity, scaling and renormalization [34, 35] and further expand upon a geometric interpretation of the fidelity[36]. The second sub-field would focus on the fidelity susceptibility and its connection, developed by You *et al.*[25], to the derivatives of the free energy and the structure factors of the Hamiltonian driving terms. These same works on the fidelity susceptibility and its relationship to the correlation functions of the system would then further confound the issue of whether the fidelity can successfully explore non-Landau-Ginzburg-Wilson type transitions. An issue which is still not resolved to this day.

3.2 Fidelity Susceptibility

A natural extension of the quantum fidelity is the fidelity susceptibility. If one expands the ground-state overlap in a differential series expansion one obtains

$$\langle \Psi_0(\lambda) | \Psi_0(\lambda + \delta\lambda) \rangle = 1 + \delta\lambda \langle \Psi_0(\lambda) | \frac{\partial \Psi_0(\lambda)}{\partial \lambda} \rangle + \delta\lambda^2 \langle \Psi_0(\lambda) | \frac{\partial^2 \Psi_0(\lambda)}{\partial \lambda^2} \rangle + \dots \quad (3.14)$$

The squared absolute value of this expression is then

$$|\langle \Psi_0(\lambda) | \Psi_0(\lambda + \delta\lambda) \rangle|^2 = 1 + \delta\lambda \left(\langle \Psi_0(\lambda) | \frac{\partial \Psi_0(\lambda)}{\partial \lambda} \rangle + \langle \frac{\partial \Psi_0(\lambda)}{\partial \lambda} | \Psi_0(\lambda) \rangle \right) + \delta\lambda^2 \left(\frac{1}{2} \langle \Psi_0(\lambda) | \frac{\partial^2 \Psi_0(\lambda)}{\partial \lambda^2} \rangle + \frac{1}{2} \langle \frac{\partial^2 \Psi_0(\lambda)}{\partial \lambda^2} | \Psi_0(\lambda) \rangle + \langle \frac{\partial \Psi_0(\lambda)}{\partial \lambda} | \Psi_0(\lambda) \rangle \langle \Psi_0(\lambda) | \frac{\partial \Psi_0(\lambda)}{\partial \lambda} \rangle \right) + \dots$$

The linear term must be zero. There are two reasons for this; firstly, due to the fact that

$$\left(\langle \Psi_0(\lambda) | \frac{\partial \Psi_0(\lambda)}{\partial \lambda} \rangle + \langle \frac{\partial \Psi_0(\lambda)}{\partial \lambda} | \Psi_0(\lambda) \rangle \right) = \frac{\partial}{\partial \lambda} \langle \Psi_0(\lambda) | \Psi_0(\lambda) \rangle \quad (3.15)$$

which must be zero since an inner-product of a state with itself is one. Another, more intuitive, reason is that if there *were* a linear term then there would be some value of λ for which the fidelity was > 1 which would be unphysical.

We then take the square-root of the above expression and expand in a power series. Since there is no linear term it is the quadratic term which is the leading term of this differential series expansion and it is this term we call the fidelity susceptibility (χ_F). Rearranging our series we get the following expression for χ_F :

$$|\langle \Psi_0(\lambda) | \Psi_0(\lambda + \delta\lambda) \rangle|^2 = 1 - \frac{(\delta\lambda)^2}{2} \chi_F$$

$$\chi_F = 2(1 - |\langle \Psi_0(\lambda) | \Psi_0(\lambda + \delta\lambda) \rangle|^2) / (\delta\lambda)^2$$

where

$$\chi_F = \left\langle \frac{\partial \Psi_0(\lambda)}{\partial \lambda} \middle| \frac{\partial \Psi_0(\lambda)}{\partial \lambda} \right\rangle - \left\langle \frac{\partial \Psi_0(\lambda)}{\partial \lambda} \middle| \Psi_0(\lambda) \right\rangle \left\langle \Psi_0(\lambda) \middle| \frac{\partial \Psi_0(\lambda)}{\partial \lambda} \right\rangle \quad (3.16)$$

(to see how this is obtained simply substitute $0 = -(\delta\lambda)^2 \frac{\partial^2}{\partial \lambda^2} \langle \Psi_0(\lambda) | \Psi_0(\lambda) \rangle$ into the series). Therefore, if $\delta\lambda$ is small but non-zero, as it is in a numerical computation, then the fidelity susceptibility is easily obtained from a measurement of the quantum fidelity. This procedure can be extended to multi-parameter Hamiltonians, however, the fidelity susceptibility then becomes a geometric tensor of the different parameters. For further information see the review by Gu[24].

3.2.1 Fidelity Susceptibility and the Derivatives of the Ground State Energy

The more traditional quantities used in determining quantum phase transitions are the first and second derivatives of the ground state energy. Therefore, it is not surprising that there is a direct link between these derivatives and the fidelity and fidelity susceptibility as was established by Chen *et al.*[37] To illustrate this connection we will first examine the case of discontinuous phase transitions.

If a discontinuous phase transition is due to a level crossing in the ground-state as discussed previously then the ground-state energy can be said to be $E_0(\lambda)$ for $\lambda < \lambda_c$ and $E_1(\lambda)$ for $\lambda > \lambda_c$; here λ_c is the critical value where the level crossing occurs and, for simplicity, it is assumed $E_0(\lambda) < E_1(\lambda)$. In this way we represent a system whose first excited state drops to a lower energy than the ground state at some value of a parameter λ . Thus we can write the ground-state energy as:

$$E_{gs}(\lambda) = \begin{cases} E_0(\lambda), & \lambda < \lambda_c \\ E_1(\lambda), & \lambda > \lambda_c. \end{cases} \quad (3.17)$$

Therefore, it follows that:

$$\frac{\partial E_{gs}(\lambda)}{\partial \lambda} = \begin{cases} \frac{\partial E_0(\lambda)}{\partial \lambda}, & \lambda < \lambda_c \\ \frac{\partial E_1(\lambda)}{\partial \lambda}, & \lambda > \lambda_c \end{cases} \quad (3.18)$$

and since, in general, $\frac{\partial E_0(\lambda)}{\partial \lambda} \neq \frac{\partial E_1(\lambda)}{\partial \lambda}$ when $\lambda = \lambda_c$ there is a discontinuity at the transition point. Thus the first-order transition is signified by a discontinuity in the first derivative of the ground-state energy. At the transition point the quantum fidelity is given by $\langle \Psi_{GS}(\lambda_c - \delta/2) | \Psi_{GS}(\lambda_c + \delta/2) \rangle$ which is $\langle \Psi_0(\lambda_c - \delta/2) | \Psi_1(\lambda_c + \delta/2) \rangle$. Therefore, as $\delta \rightarrow 0$, $\langle \Psi_0(\lambda_c) | \Psi_1(\lambda_c) \rangle$ will be much less than one (possibly even 0 if the two states are orthogonal). Since $\langle \Psi_0(\lambda) | \Psi_0(\lambda) \rangle$ and $\langle \Psi_1(\lambda) | \Psi_1(\lambda) \rangle$ will be very, very close to 1 in their respective regions, a discontinuous transition will be indicated by a sudden and sharp drop in the quantum fidelity from 1 to some lower value and back to 1. Through this behaviour the quantum fidelity, which spikes downward at a discontinuous transition, is connected to the first derivative of the ground-state energy, which has a discontinuity at the same point.

Next we will consider second-order transitions. In the previous section we defined the fidelity susceptibility by expanding the ground-state in a power series. However, we can also expand it perturbatively. Doing this, to first order, it becomes

$$|\Psi_0(\lambda + \delta\lambda)\rangle = c(|\Psi_0(\lambda)\rangle) + \delta\lambda \sum_{n \neq 0} \frac{H^{n0} |\Psi_n(\lambda)\rangle}{E_0(\lambda) - E_n(\lambda)} + \dots \quad (3.19)$$

where $H^{n0} = \langle \Psi_n(\lambda) | H_I | \Psi_0(\lambda) \rangle$ and H_I comes from $H = H_0 + \lambda H_I$ as discussed previously (c is a normalization constant). We assume here that the ground-state is non-degenerate (i.e. continuous phase transitions). With a little algebra this can be normalized and by acting on it from the left with $\langle \Psi(\lambda) |$ we can write this in terms of the fidelity to get

$$F(\lambda)^2 = 1 - \delta\lambda^2 \sum_{n \neq 0} \frac{|H^{n0}|^2}{[E_0(\lambda) - E_n(\lambda)]^2} + \dots \quad (3.20)$$

Therefore, by matching terms with the power series definition discussed previously we see that the fidelity susceptibility is

$$\chi_F = \sum_{n \neq 0} \frac{|H^{n0}|^2}{[E_0(\lambda) - E_n(\lambda)]^2}. \quad (3.21)$$

Now, if we remember our basic quantum mechanics the second-order perturbation of the energy is

$$E_0^{(2)} = \sum_{n \neq 0} \frac{|H^{n0}|^2}{[E_0(\lambda) - E_n(\lambda)]} \quad (3.22)$$

which differs from the fidelity susceptibility only by the exponent of the denominator. Thus, the fidelity susceptibility goes to infinity *faster* than the second derivative of the ground-state energy and therefore can be said to be a finer and more precise measure of second-order transitions.

The similarities between the quantum fidelity and the fidelity susceptibility and the first and second derivatives of the ground-state energy may make one wonder what is the value of the fidelity approach. If it can only detect transitions that can also be detected by the ground-state energy then it can't really contribute anything new to the field of quantum phase transitions.

3.2.2 Fidelity Susceptibility and Dynamic Structure Factors; A Connection

Another insight into the nature of the fidelity susceptibility was gleaned by Gu et al.[25] They began by defining a related quantity called the *dynamic fidelity susceptibility*:

$$\chi_F(\omega) = \sum_{n \neq 0} \frac{|H^{n0}|^2}{[E_0(\lambda) - E_n(\lambda)]^2 + \omega^2} \quad (3.23)$$

which can be Fourier Transformed into

$$\chi_F(\tau) = \sum_{n \neq 0} \frac{\pi |H^{n0}|^2}{[E_0(\lambda) - E_n(\lambda)]^2} e^{-(E_n - E_0)|\tau|}. \quad (3.24)$$

They then showed that this transformed dynamic susceptibility was related to the dynamic structure factor of the driving Hamiltonian by the relation

$$\frac{\partial \chi_F(\tau)}{\partial \tau} = -\pi [\langle \Psi_0 | H_I(\tau) H_I(0) | \Psi_0 \rangle - \langle \Psi_0 | H_I | \Psi_0 \rangle^2] \theta(\tau) + \pi [\langle \Psi_0 | H_I(0) H_I(\tau) | \Psi_0 \rangle - \langle \Psi_0 | H_I | \Psi_0 \rangle^2] \theta(-\tau) \quad (3.25)$$

where

$$H_I(\tau) = e^{H(\lambda)\tau} H_I e^{-H(\lambda)\tau} \quad (3.26)$$

and $\theta(\tau)$ is the step-function. This can also be rewritten as

$$\chi_F(\tau) = \int_0^\infty \tau G_I(\tau) d\tau \quad (3.27)$$

where

$$G_I(\tau) = \langle \Psi_0 | H_I(\tau) H_I(0) | \Psi_0 \rangle - \langle \Psi_0 | H_I | \Psi_0 \rangle^2. \quad (3.28)$$

This expression is very close to the expression

$$E_0^{(2)} = \int \langle \Psi_0 | H_I(\tau) H_I(0) | \Psi_0 \rangle - \langle \Psi_0 | H_I | \Psi_0 \rangle^2 \quad (3.29)$$

for the second-order perturbation of the ground-state energy. Thus we see another way in which the fidelity susceptibility is connected to the derivatives of the ground-state energy and the relation with $\frac{\partial \chi_F(\omega, \tau)}{\partial \tau}$, again, suggests that it may be a more sensitive alternative.

3.2.3 The Fidelity Susceptibility and Higher-Order Transitions

The obvious question with regard to the quantum fidelity and fidelity susceptibility is whether they can detect phase transitions which are difficult or impossible to identify via other methods (such as the derivatives of the ground-state energy). Examples of such transitions are: higher-order transitions; infinite-order transitions (BKT-type); and topological transitions.

As was previously shown the perturbative expression of the fidelity susceptibility

$$\chi_F = \sum_{n \neq 0} \frac{|H^{n0}|^2}{[E_0(\lambda) - E_n(\lambda)]^2}. \quad (3.30)$$

differs from the second derivative of the ground-state energy only by the power of the denominator. This means that though the fidelity susceptibility will diverge in all situations

where the second derivative of the ground-state energy will it may also diverge in other situations. Therefore, whether or not the fidelity susceptibility diverges for, say, third-order transitions is difficult to determine. However, one would not expect the fidelity susceptibility, in general, to be a good probe of third-order and higher transitions.[24] Though, one could always consider higher-order fidelity susceptibilities for such situations.

When the fidelity susceptibility was previously derived it was via a series expansion to first-leading-term only. One need not stop there, one could easily define a second-order fidelity susceptibility that arises from the second-leading-term and one for the third-leading-term and so on. The procedure for defining such higher-order fidelity susceptibilities will not be discussed here but can be found in the references.[24] However, whether or not these higher-order fidelity susceptibilities have any advantage over the more traditional ground-state energy derivatives is still largely unknown.

Whether or not the fidelity susceptibility can be used to identify BKT transitions, being transitions of infinite order, is still hotly debated.[24, 37, 38] In this work a BKT-type transition will be detected in the Heisenberg Next-Nearest-Neighbour Spin Chain using a new type of fidelity susceptibility which will be introduced shortly. That particular transition in the Heisenberg Spin Chain was also accurately determined by Chen *et al* using the quantum fidelity (not the fidelity susceptibility) by considering a level-crossing in the *first-excited state* rather than the ground-state.[26] However, in a later paper Chen *et al* would claim that for “the KT transition the criticality is not a sufficient condition to ensure divergence of the FS (Fidelity Susceptibility)”.[37].

Yet, despite disagreement over whether the fidelity susceptibility can, in general, identify BKT-type transitions specific BKT transitions have been successfully detected in the XXZ model[38] and the one-dimensional Hubbard model[39]. Therefore, it is safe to say that the relationship between the fidelity susceptibility and BKT transitions is still poorly understood.

The issue as to whether topological phase transitions are detectable by a fidelity susceptibility approach is also unclear. Preliminary work using variants of the Kitaev model have shown that the fidelity, in some cases at least, can identify topological phase transitions. Specifically, topological transitions have been correctly identified in the honeycomb Kitaev model[40] by Yang *et al* and in the deformed Kitaev toric model[41] by Abasto *et al*. These early successes demonstrate that a fidelity approach shows promise as a probe of topological transitions. However, the exact reason *why* the fidelity susceptibility is able to detect such transitions is still something of a mystery. Thus, as of yet there is little that can be concluded about the general effectiveness of fidelity approaches when considering topological behaviour. Like the other more exotic transitions the issue is still hotly debated.

4 The Heisenberg Next-Nearest Neighbour Spin Chain

The Heisenberg Next-Nearest Neighbour Spin Chain (a.k.a. the J_1 - J_2 model) is a simple system which displays comparatively rich physics. Most importantly, it exhibits a BKT-type transition. Despite having a relatively simply Hamiltonian of the form

$$H = J_1 \sum_{\langle i,j \rangle} \vec{S}_i \cdot \vec{S}_j + J_2 \sum_{NNN} \vec{S}_i \cdot \vec{S}_j \quad (4.1)$$

no analytical solution exists for general values of J_2 , though solutions are known for specific J_2 values. In the limit of $J_2 = 0$ the model reduces to a Heisenberg Spin Chain whose exact solution can be found via the Bethe Ansatz[42, 43]. For $J_2 = 1/2$ the system becomes the well studied Majumdar-Ghosh model whose ground-state is known to be an equally weighted superposition of nearest-neighbour valence bond states (dimers).[44]

In fact, even though there exists no exact solution to the $J_1 - J_2$ model a great deal is known about its ground-state as a function of J_2/J_1 . It has been studied by: analytical methods, such as Bosonization[45] and Effective Field Theory[46]; Exact Diagonalization methods[47, 48]; and via Density Matrix Renormalization Groups (DMRG)[49, 50, 51]. From these DMRG analyses it is known that for J_2/J_1 s less than some $(J_2/J_1)_c$ the frustration introduced by the next-nearest-neighbour interaction J_2 becomes irrelevant and the system renormalizes to the Heisenberg fixed point whose ground-state is known to be a spin liquid or Luttinger liquid with massless spinon excitations. Conversely, when $J_2/J_1 > (J_2/J_1)_c$ the J_2 term becomes a relevant interaction and the system renormalizes to a dimerized ground-state with a spin gap. Between the spin liquid and dimerized phases there is a known BKT transition and from the previously mentioned Effective Field Theory studies its position is known quite accurately to be $J_2/J_1 = 0.2411676 \pm 0.000005$. [46, 48] This transition value has been verified to a precision of $J_2/J_1 = 0.2411 \pm 0.0001$ through Conformal Field Theory methods.[52, 53] However, in general the $J_1 - J_2$ transition point is notoriously difficult to identify due to logarithmic correction.[54]

The $J_1 - J_2$ model's simplicity and the accuracy to which its BKT transition is known make it an ideal model for validation of new methods. Therefore, it will be on this model that the method introduced in this work, the CFFS, will be initially applied. Since, our primary interest is in the BKT transition only the region $J_2/J_1 < 0.5$ will be considered.

4.1 The Conjugate Field Fidelity and Fidelity Susceptibility

Before introducing the Conjugate Field Fidelity Susceptibility (CFFS) it may be prudent to briefly introduce, for those unfamiliar, the *conjugate field*. The conjugate field is defined as a field which couples linearly to the variable whose expectation value is the order parameter.[55] It could also be described as the specific external force which breaks the degeneracy of ground-states in a phase transition. It is from this notion of a conjugate field that one can alternately define the order-parameter-susceptibility as the linear response of the order parameter to an infinitesimal conjugate field:

$$\chi = \left. \frac{\delta \Phi}{\delta h} \right|_{\delta h \rightarrow 0} \quad (4.2)$$

where Φ is the order parameter and h is the conjugate field. As the order parameter of a system changes from zero to a finite numbers through phase transition the order-parameter-susceptibility diverges to infinity. We are perhaps most familiar with these concepts in the case of ferromagnetic system where the conjugate field is simply the external z field h_z which is linearly coupled to the magnetization ($\langle \sum_i S_i^z \rangle$). The order-parameter-susceptibility in that case is imply the magnetic susceptibility. For a further review of the order-parameter-susceptibility and its relation to a conjugate field one is referred to a graduate-level statistical physics textbooks such as those by Reichl[56] and Huang[57].

The CFFS is a very similar quantity to the order-parameter-susceptibility. To construct it, first one assumes an order parameter exists, be it local or global, and defines a conjugate field which is linearly coupled to it. The CFFS is then the fidelity susceptibility associated with a slightly different kind of quantum fidelity called the *Conjugate Field Fidelity*. The normal quantum fidelity is the absolute overlap between the ground-state of a system and the ground-state of the same system when a system parameter is perturbed, i.e.

$$F(\lambda, \delta\lambda) = |\langle \Psi_{gs}(\lambda) | \Psi_{gs}(\lambda + \delta\lambda) \rangle|. \quad (4.3)$$

The conjugate field fidelity is the absolute overlap between the ground-state of a system and a system which has been perturbed *by an infinitesimal conjugate field*, i.e.

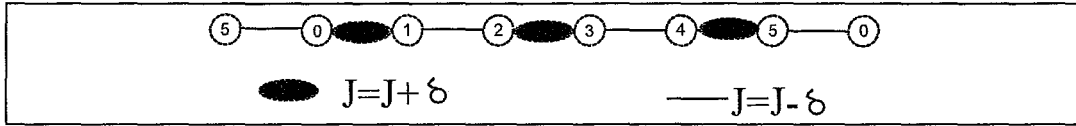


Fig. 2: This diagram shows how the Hamiltonian is perturbed when constructing χ_D . The thick bonds have a bond strength of $J + \delta J$ and the thin bonds have a strength $J - \delta J$. This perturbs the Hamiltonian such that dimerized states have lower energy.

$$\text{conjugate field fidelity} = F_{CF}(h, \delta h) = |\langle \Psi_{gs}(\lambda) | \Psi_{gs}(\lambda + \delta h) \rangle|. \quad (4.4)$$

where h is a conjugate field for some order parameter. Obtaining the Conjugate Field Fidelity Susceptibility from the Conjugate Field Fidelity is then straightforward (see Section 3.2):

$$\text{conjugate field fidelity susceptibility} = \chi = 2(1 - F_{CF})/\delta h^2 \quad (4.5)$$

The rationale of the CFFS is simple, if the system of interest is in a phase characterized by the given order parameter from which the conjugate field was derived then the CFFS will diverge (in the limit of an infinite system size). If the system is not in said phase then the CFFS will not. The attractiveness of such a quantity is that if one is unsure as to whether a given system is in one phase or another for some particular values of the Hamiltonian parameters then one can construct a *separate* CFFS for each phase. If we say there are two possible phases a given system could be in, *phase 1* or *phase 2* then one can determine the conjugate field for each phase (which will be different) and construct two conjugate field fidelity susceptibilities, χ_1 and χ_2 . In the limit of infinite system size the CFFS corresponding to the phase the system is in will diverge, the other will not. In as much as the conjugate field represents the fluctuations of the order parameter with respect to a specific type of order, the CFFS allows one to infer which types of fluctuations are dominating for a given set of system parameters. The assumption being that the system can be said to be *in* the phase for which the fluctuations of that phases order parameter are the largest. To make the concept of the CFFS more clear we will now apply it to the $J_1 - J_2$ model.

4.2 The Dimerized Susceptibility

In the $J_1 - J_2$ model we are interested in whether the CFFS method can do two things: firstly, can it identify, given a value of J_2/J_1 , whether the system is in the Luttinger liquid phase or the dimerized phase; secondly, can it accurately determine the value of J_2/J_1 where this transition occurs. The first step in applying the CFFS technique is to identify conjugate fields for the phases of interest. However, since there is no simple way to implement an order parameter that can characterize a Luttinger liquid a slightly different tact will be taken.

From previous work on the $J_1 - J_2$ model it is known that the two dominant phases are the critical (Luttinger) liquid and dimer phases. Therefore, if the system is not in the dimer phase it is in the liquid phase. Thus, one only need to construct a CFFS for the dimer phase and then the other phase can be inferred as the region of parameter space for which the system is not dimerized. To this end we define the *dimerized susceptibility* (χ_D).

The dimerized susceptibility, χ_D , stems from a dimerized conjugate field which promotes dimerized order (see Fig. 2). The $J_1 - J_2$ Hamiltonian after being perturbed by the dimerized conjugate field has the form

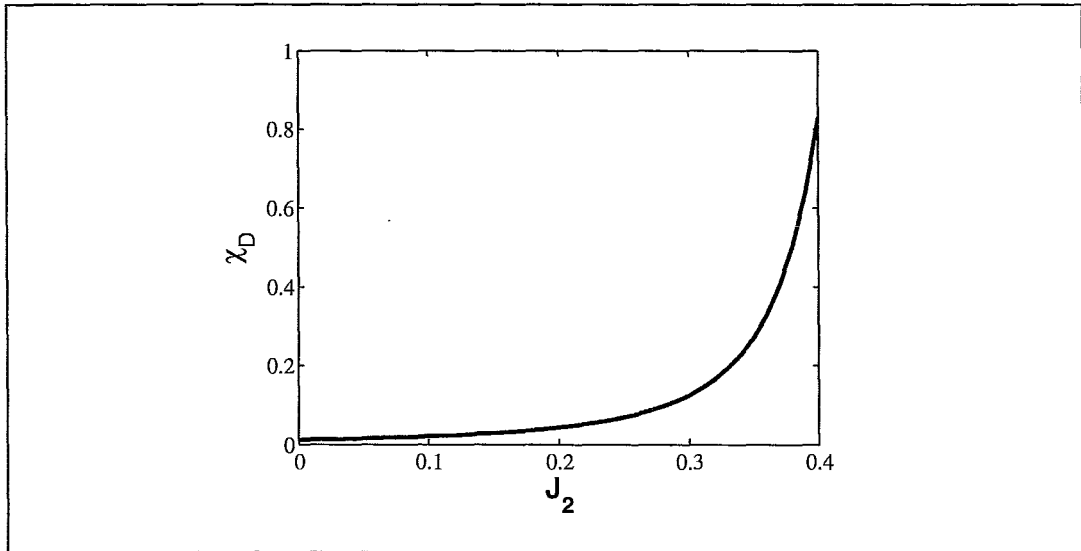


Fig. 3: χ_D vs. J_2 . Notice the rise to infinity. In the limit of infinite system size this divergence would occur at the transition point. ($L=16$)

$$H(J_1, J_2, \delta h) = J_1 \sum_{i=1}^L (\vec{S}_i \cdot \vec{S}_{i+1} + (-1)^i \delta h) + J_2 \sum_{i=1}^L \vec{S}_i \cdot \vec{S}_{i+2} \quad (4.6)$$

where periodic boundary conditions are assumed ($S_{L+1} = S_1$). Initially the form of the Hamiltonian may seem odd but its physical interpretation is intuitive. With the conjugate field perturbation a ground-state which has a specific pattern of dimerization will have a slightly lower energy. Using this χ_D we can now apply the CFFS method to the $J_1 - J_2$ model.

4.3 Method and Results

In order to compute χ_D a δh of between 0.001 and 0.00001 was used. The variation in δh is due to the fact that too small a δh will cause smaller systems to become numerically unstable. Therefore, the smallest possible value of δh that did not produce erratic results was used to maximize accuracy. In all calculations periodic boundary conditions were applied.

Computing χ_D for a sample chain (see Fig. 3) we see that its value is initially small and then as J_2 increases it grows exponentially. This is consistent with what we would expect to see. For a system of infinite size we expect an asymptote at the transition point due to χ_D 's relation to the order-parameter-susceptibility which will be infinite in the phase characterized by that order-parameter. For a finite system this manifests as an exponential divergence.

Once χ_D was computed for the system sizes $L=8,10,12,\dots,30$ graphs of χ_D/L^3 were plotted. The reason for the increase in system size by 2 is due to the fact that 2 sites must be added (not just 1) in order to make a dimer covering that obeys periodic boundary conditions. The intersection between those curves and the curves of the next largest system (i.e. the intersection of χ_D/L^3 and $\chi_D/(L+2)^3$) were then tabulated (for a sample intersection see Fig. 4). At this point it is prudent to discuss the L^3 scaling of the system.

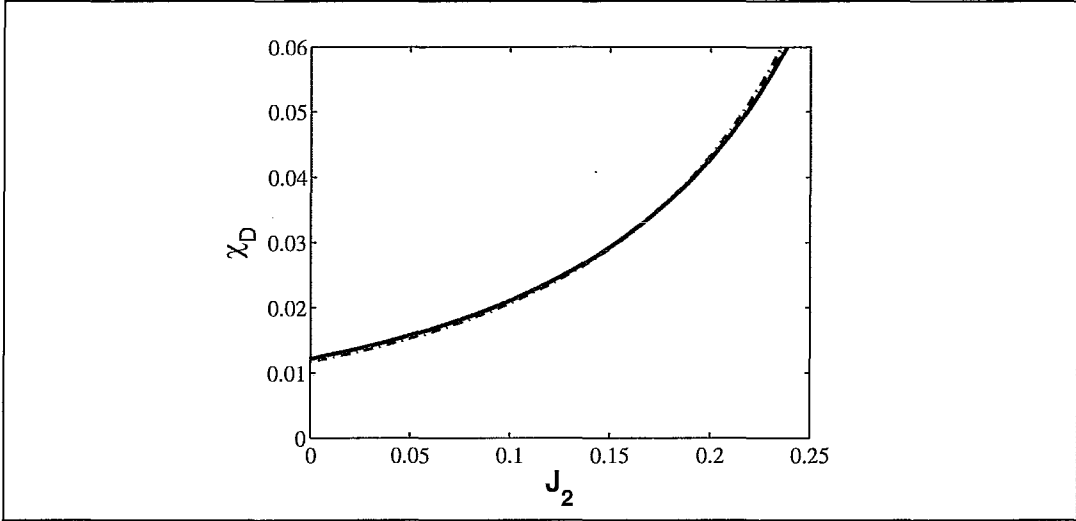


Fig. 4: This graph shows the intersection of χ_D/L^3 vs. J_2 for system sizes of $L = 12$ (solid line) and $L = 14$ (dashed line). The intersection is difficult to see due to the closeness of the two curves. In the limit of infinite system sizes this intersection will tend to the transition point.

4.3.1 Scaling of the Fidelity Susceptibility

From work by Zenuti and Zanardi[58] it is known that the fidelity susceptibility scales as

$$\chi_D \propto L^{2d+2\zeta-2\Delta_V} \quad (4.7)$$

where d is the dimensionality, ζ is the dynamic exponent and Δ_V is the scaling dimension of the driving operator in the Hamiltonian. The $J_1 - J_2$ chain is in the same universality class as a $c = 1$ conformal field theory and thus $d = 1$ and $\zeta = 1$. It is also known that the scaling dimension of the dimerization operator is $1/2$. Therefore, for the spin-1/2 chain we expect χ_D to scale as

$$\chi_D \propto L^{2(1)+2(1)-2(\frac{1}{2})} \propto L^3. \quad (4.8)$$

To confirm this L^3 dependency a scaling analysis was performed at three points; below the critical point ($J_2 = 0.1$), at the critical point ($J_2 = 0.241167$) and above the critical point ($J_2 = 0.4$). At these three values χ_D was calculated as a function of system size and then fitted with a line of best fit. In the Luttinger critical phase $J_2 = 0.1$ the data best fit to a power-law of exponent ~ 2.81 (the importance of this discrepancy in the non-critical region will be discussed in more detail later). In the dimerized phase $J_2 = 0.4$ the data was found not to fit a power-law at all but an exponential (see Fig. 5a). At the critical point $J_2 = 0.241167$, χ_D was found to fit a power-law with exponent ~ 3.02 (see Fig. 5b). This scaling analysis strongly supports the theoretically predicated scaling of $\propto L^3$ and thus this is the scaling correction that was used.

4.3.2 Results (cont.)

By analysing the intersection points of χ_D/L^3 for increasingly longer chains we see that they do not all cross at the same value. This is due to correction to scaling by lower order terms in finite-size scaling. Thus, the intersection points as a function of system size were fitted with a power-law (See Fig. 6). This power-law (with exponent ~ -1.82) was found to

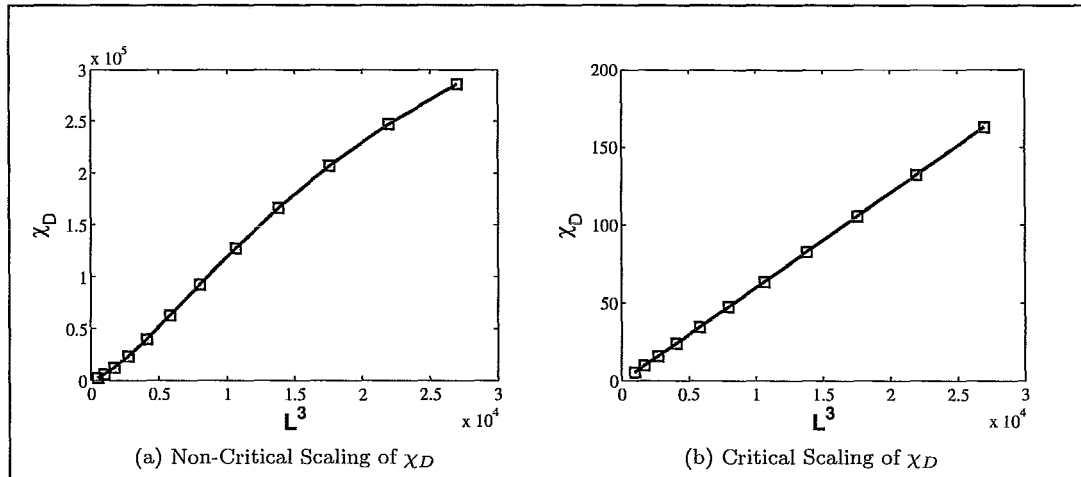


Fig. 5: *Left: The scaling of χ_D vs. L^3 in the dimerized region ($J' = 0.4$). Notice the non-linear fit. This is due to exponential scaling in this region. Right: The scaling of χ_D vs. L^3 at the critical point. Notice the excellent fit.*

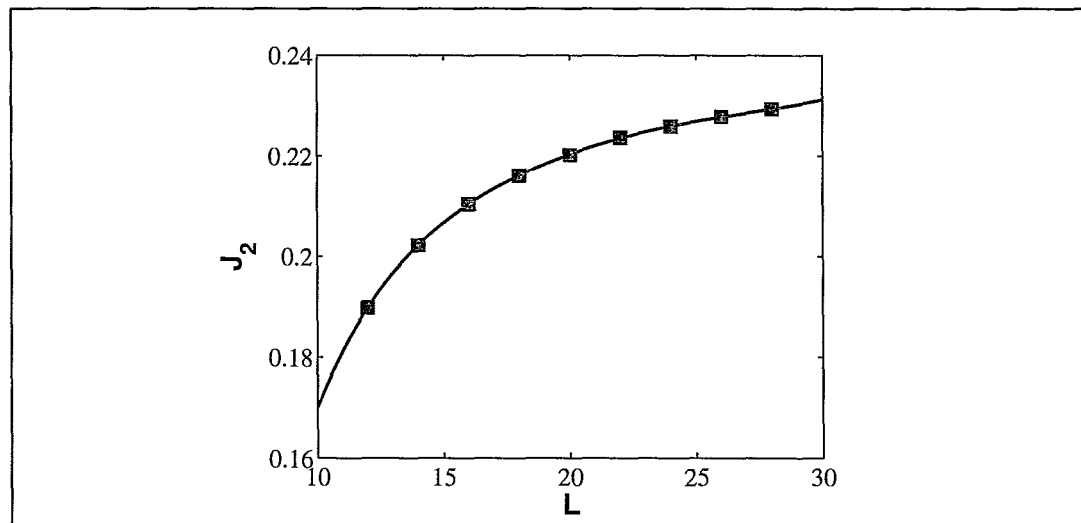


Fig. 6: *This graph shows the power-law fitting of the χ_D/L^3 intersection points. In the limit of $L = \infty$ the line of best fit is found to converge to $J_2 = 0.241$. This is in excellent agreement with other theoretical results.*

be in excellent agreement with the data and extrapolation to the limit of $L = \infty$ produced an intersection point of $J_2 = 0.24$. This is in very good agreement with the expected value of 0.2411676[48].

4.4 Discussion

Although the CFFS method has proven successful at identifying the BKT-type transition in the spin-1/2 chain, whether or not it can, in general, describe infinite-order transitions is still unclear. It's possible some fortuitous scaling properties of the spin-1/2 chain may have allowed a determination to be made in this particular case but not in others. From work by Affleck *et al.*[54] it is known that the spin-1/2 chain scales with logarithmic corrections.

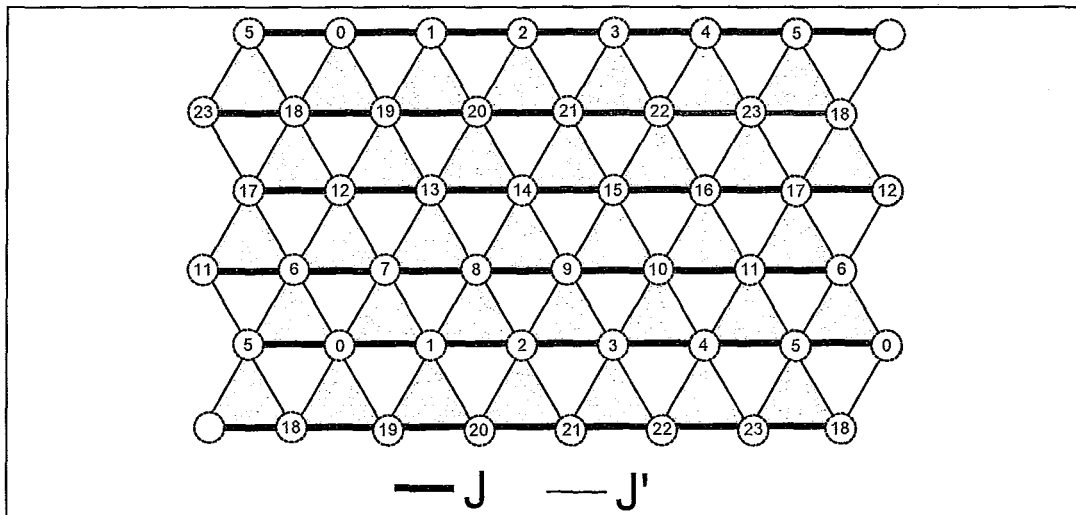


Fig. 7: The anisotropic triangular lattice. Thin lined diagonal bonds have strength J' . Thick lined horizontal bonds have a strength of J and a second-nearest neighbour interaction of J_2 . In the limit of $J' \ll J$ this system behaves as a set of loosely couple spin chains.

These logarithmic corrections to finite-sized scaling makes it difficult to glean accurate information with only the small system sizes available from an exact diagonalization study. However, at the transition point, a marginal operator produces couplings which vanish under renormalization (i.e. they are relevant on one side of the transition and irrelevant on the other). Thus, at the critical point in the spin-1/2 chain there are no logarithmic corrections and thus the critical point has a simple scaling factor of 3 and can be estimated by looking at relatively large systems and extrapolating using a power law. If the system had logarithmic corrections to scale that did not vanish at the transition point then the CFFS method would be significantly less effective at numerically estimating it. However, as it stands the CFFS has been shown to successfully arrive at the expected critical value of $J_2 = 0.24$.

5 The Anisotropic Triangular Model

5.1 An Introduction; Cs_2CuCl_4

Studies of the two-dimensional spin-1/2 Heisenberg triangular model are pervasive in Condensed Matter physics, however the anisotropic variant has only recently begun to gather attention. In essence, the Heisenberg Anisotropic Triangular Model (HATM) generalizes the standard triangular lattice Hamiltonian

$$H = J_1 \sum_{NN} \vec{S}_i \cdot \vec{S}_j + J_2 \sum_{NNN} \vec{S}_i \cdot \vec{S}_j \quad (5.1)$$

by allowing the bond strength of diagonal exchange interactions to vary (see Fig. 7).

Thus, the HATM's Hamiltonian has three parameters, the horizontal nearest-neighbour interaction J , the horizontal next-nearest-neighbour interaction J_2 and the diagonal interaction J' . We can then see that when $J' \ll J$ the system behaves as a series of nearly independent Heisenberg spin chains that are only loosely coupled by a diagonal interaction J' . It is important to note that there is *no* second-nearest-neighbour interaction along the diagonal or between loosely coupled chains, only along the horizontal.

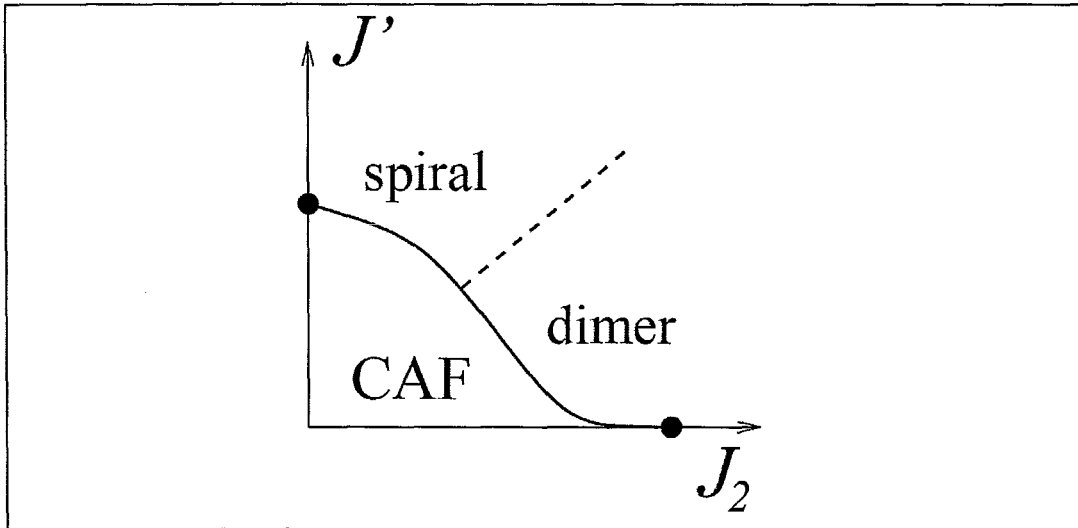


Fig. 8: The phase diagram of the HATM as suggested by Balents *et al.*[70]

It is to the recent observations of a strong inelastic continuum in neutron scattering of the quasi-1D inorganic salt Cs_2CuCl_4 [61] that the HATM owes its new popularity. These scattering results are characteristic of a *resonating-valence-bond (RVB) state*[62] and thus suggest that Cs_2CuCl_4 may exhibit a *two-dimensional spin-liquid phase*. [63, 64, 65] Spin-liquid states are of immense current interest and the potential discovery of an experimental example is extremely noteworthy.

That brings us to the HATM which is believed to be a good theoretical model of Cs_2CuCl_4 with a J'/J value of 0.34.[66] Thus, an exploration of its phase diagram is not only theoretically interesting but could potentially shed light on a substance that displays a real spin-liquid phase. Previously, the phase diagram of the HATM has been studied by means of semiclassical spin-wave calculations[67, 68, 69] and a Renormalization Group (RG) analysis by Balents *et al.*[70, 71, 72]. From these works a rough, and somewhat contentious, outline of the HATM phase diagram has been discerned.

5.2 The Proposed Phase Diagram $J_2 = 0$

With the strong interest in Cs_2CuCl_4 has come much numerical work. However, most of this work has been confined to the region $J_2 = 0$ (first-nearest-neighbour only). DMRG work by Weng *et al.*[73] as well as Variational Wavefunction and Monte-Carlo work by Sorella *et al.*[74, 75] have suggested a phase diagram for this particular case. Their findings suggest that the HATM exhibits a 1D spin liquid phase in the approximate region $J' = 0.0 - 0.6$, a 2D spin liquid phase for $J' = 0.6 - 0.85$ before entering a spirally ordered phase. However, other Renormalization Group work by Balents *et al.*[76] as well as numerical coupled cluster calculations by Campbell *et al.*[77] suggest that subtle fourth-order fluctuations push the HATM into a collinear antiferromagnetically ordered phase instead for small values of J'/J . The direct relation of these fourth-order fluctuations to the actual phase of Cs_2CuCl_4 is still largely unknown.[78]

5.3 The Proposed Phase Diagram $J_2 \neq 0$

The proposed phase diagram of the HATM, for $J_2 \neq 0$ contains three distinct extremes (See Fig. 8). For small values of J'/J (i.e. loosely interacting spin-chains) the system

is known to be in competition between a magnetically ordered collinear-antiferromagnetic (CAF) phase and a dimerized phase. When the next-nearest-neighbour exchange interaction is weak (J_2/J is small) the CAF wins out and for larger values of J_2/J the system is in a dimerized phase. For the trivial case of $J' = 0$ (i.e. completely uncoupled spin-1/2 chains) the phase diagram is well known (and confirmed early in this work); the system is in a (Luttinger) critical state until $J_2/J = 0.24$ before it spontaneously dimerizes. However, the transition point between the CAF and dimerized phases for non-zero J' has not been quantitatively established in any published work (that this author knows of).

The final sector of the HATM phase diagram occurs at the limit of large J'/J . In the specific case of $J'/J = 1$, $J_2 = 0$ the system reverts to the ordinary spin-1/2 triangular model which is known to exhibit a strong, geometrical 120° spiral ordered phase.[79] For non-zero values of J_2 and $J' < J$ the system will not have a perfect 120° spiral ordering, however, it is believed that for $J' \sim J$ the system is still ordered *spiral-like*. [80] Again, there exists no quantitative estimate of the transition curve between CAF ordering and spiral-ordering nor of the transition curve between spiral-ordering and dimerization which must also exist. It is with this state of affairs that we begin our own analysis using the CFFS method to confirm the proposed phase diagram.

5.4 The Susceptibilities

In order to investigate the three proposed phases of the HATM we must first construct three distinct susceptibilities. These susceptibilities will be discussed now.

5.4.1 The Dimerized Susceptibility

The first susceptibility that will be used is simply the dimerized χ_D from before extended to two-dimensions. With the introduction of a second dimension the degeneracy of possible dimer coverings increases exponentially with each new added coupled spin-chain (for each new row there are 2 possibilities thus there are $2^{\text{number of rows}}$ possible configurations). However, symmetry arguments can be used to disqualify most of these as potential ground-states leaving only two types remaining, *columnar* coverings and *staggered* coverings. In this work staggered coverings are assumed when discussing χ_D in keeping with the literature, but for the sake of thoroughness all data was also generated using columnar coverings with negligible effect to results.

The dimerized susceptibility χ_D is obtained by perturbing the Hamiltonian in such a way that it promotes dimer order (see Fig. 9). Its Hamiltonian is the same as that for the spin-1/2 chain studies previously.

5.4.2 The Collinear-Antiferromagnetic (CAF) Susceptibility

The CAF CFFS χ_{CAF} is constructed by perturbing the system towards CAF order through the application of a small external field δh (See Fig. 10). The perturbed Hamiltonian thus becomes

$$H = \sum_{\langle i,j \rangle} J_{ij} \vec{S}_i \cdot \vec{S}_j + \delta h \sum_{i=1}^N (-1)^i S_z \quad (5.2)$$

with the external h field flipping directions every other spin in an antiferromagnetic-like pattern. It is worth noting that, by adding an external field aligned along the z -axis, spin-inversion symmetry is broken and thus cannot be used to help compute this susceptibility.

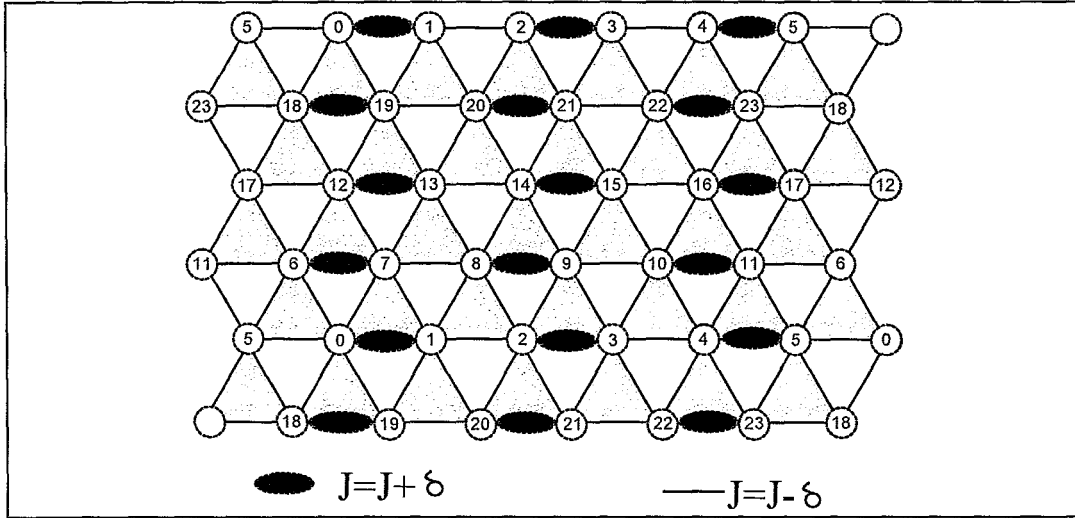


Fig. 9: A diagram of the Hamiltonian perturbation which forms the dimerized susceptibility χ_D . This generalizes the one-dimensional case to two-dimensions.

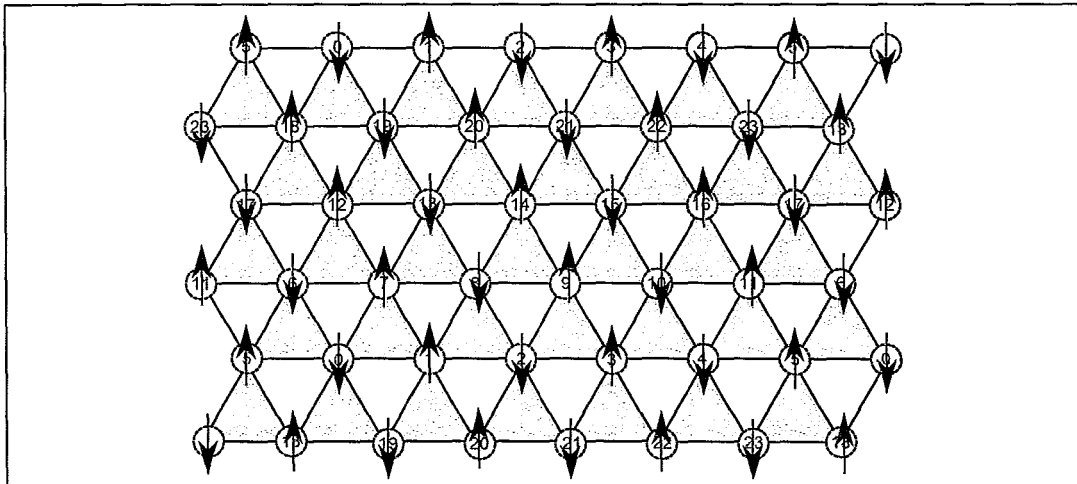


Fig. 10: A diagram of the Hamiltonian perturbation which forms the CAF susceptibility χ_{CAF} . The arrows represent the orientation of an external field δh . An up arrow indicates that that site experiences a field of $+\delta h$. A down site indicates $-\delta h$.

5.4.3 The Spiral Susceptibility

The final CFFS used here is the spiral susceptibility χ_S . Although the system is not expected to show true 120° spiral-order unless $J = J'$, the ordering is still believed to be spiral-like for a region of the phase diagram. Thus, we posit that a susceptibility coupled to the order parameter of a 120° spiral ordering will still show a dominant signal in this spiral-like region; as will be seen, this assumption seems to be justified.

It is quite laborious to include an external field for each site as was done for χ_{CAF} since coding an external field with an S_x or S_y component is quite difficult to do while maintaining the various hard-coded symmetries and Hamiltonian reduction techniques. Thus, only the sites with spins aligned along the z -axis in the 120° spiral order will be perturbed with a field yielding the Hamiltonian

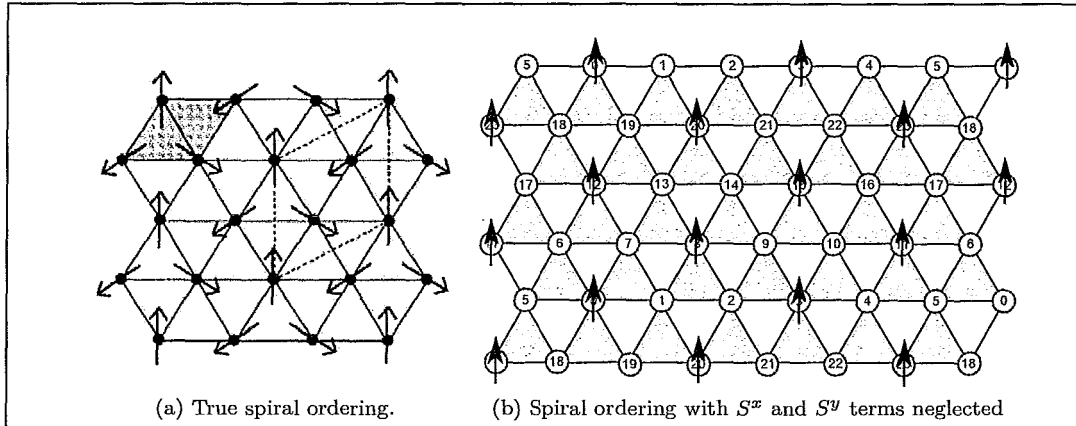


Fig. 11: *Left: A diagram of true 120° -spiral order. Right: A diagram of the Hamiltonian perturbation which forms the spiral susceptibility χ_S . Field terms with S^y or S^x components are neglected (diagonal fields) due to the difficulty to program. Notice that the patterning is distinct from that of χ_{CAF} and thus they do not overlap.*

$$H = \sum_{\langle i,j \rangle} J_{ij} \vec{S}_i \cdot \vec{S}_j - \delta h \sum_{i=1}^N \epsilon_i S_z \quad (5.3)$$

where ϵ_i is zero unless i is a multiple of 3, then it is 1. A diagram of this conjugate field can be seen in Fig. 11 where it can be seen that, though the spiral conjugate field contains only z -axis fields like the CAF, the arrangement is unique to χ_S and thus χ_S and χ_{CAF} indicate entirely separate orderings.

5.5 The Method

Our approach to the HATM will differ from that used for the Heisenberg Spin Chain. In the Spin Chain we were attempting to numerically determine the exact transition point between the Luttinger Liquid phase and the dimerized phase, here, we will expand upon the CFFS method and attempt to use it to confirm the speculative phase diagram presented in the literature. Thus, we are less interested in the *exact* curves in phase space which distinguish the three phases but more in confirming the existence of these phases as well as transitions between them. To this end we adjust our strategy and propose a new use for the CFFS.

When the HATM system is in a given phase, say the dimerized phase, then perturbations of the Hamiltonian that promote dimerized order (like those used in χ_D) will affect a significantly larger change in the ground-state than a perturbation that is not coupled in any way to the order parameter of the dimer state (like perturbations towards spiral-order). Thus, it is our contention that, while in the dimer phase, χ_D will exhibit a strong signal where χ_S and χ_{CAF} will have virtually no signal. Therefore, by comparing the relative magnitudes of the three susceptibilities we conclude that the system is in, for a certain value of J , J' and J_2 , whichever phase corresponds to the susceptibility with the largest magnitude. However, things are not so simple.

The difficulty in comparing the relative magnitudes of the susceptibilities is that it is somewhat fallacious. For one, when designing the conjugate field susceptibility the magnitude of the applied perturbations was not standard. For χ_{CAF} , each site was given either a positive or negative perturbation of size δ , which in numerical simulation is not vanishingly small, thus, for a system of size 24, that's 24 perturbations, whereas in χ_D a perturbation

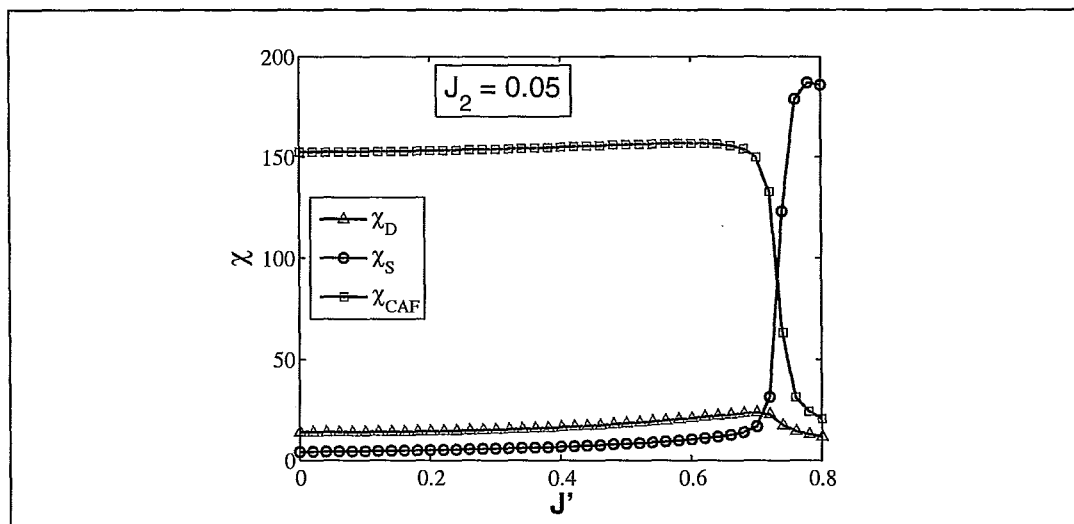


Fig. 12: This diagram shows a vertical cross-section of the HATM phase diagram ($J_2 = 0.05$). Notice the initial domination of χ_{CAF} in the region $J' = 0.0 \dots 0.7$ at which point χ_{CAF} diminishes to nothing and χ_S spikes. We would take this as a strong indication of a transition from CAF ordering to spiral ordering.

of size δ was only applied for every *other* site and thus only 12 perturbation; for χ_S only every third site. How the disparity in the numerical size of these perturbations correlates to the height of the corresponding susceptibility is unknown. Furthermore, when constructing our perturbations we only perturb towards a single possible ordering, there are in reality degenerately many. There are, in fact, *more* possible ways to construct a dimer covering than a spiral, for example. How these degeneracy issues effect the susceptibilities is again unknown. There are other reasons why comparing these susceptibilities on equal footing is treacherous (such as the lack of true 120° spiral ordering until $J = J'$). However, as we will see these issues end up only causing complications in one region of the phase diagram. These issues of relative magnitude also mean that the numerical crossing of two susceptibilities (i.e. when the height of one susceptibility overtakes another) cannot be said to be a remotely accurate estimate of the actual transition point.

5.6 The Results

Using a δh of 0.0001 and a system size of 24 the HATM phase diagram was investigated by means of cross-sections using the CFFS method. A sample vertical cross-section can be seen in Fig. 12, where J_2 was taken as a constant 0.005 and J' was varied for a J of 1. For reference, the typical fidelity susceptibility for this region is also shown in Fig. 13. For small values of J'/J χ_{CAF} is clearly dominant over χ_S and χ_D confirming CAF ordering in this region. However, at $\sim J'/J = 0.76$ χ_{CAF} suddenly plummets. We would take this, and the sudden rise of χ_S to indicate a transition to spiral-order. Notice that the difference in relative magnitudes becomes huge after this transition point, effectively quashing any concerns over the comparison of magnitudes of these susceptibilities.

If we now look at a horizontal cross-section taken with a constant J' of 0.005 and varied J_2/J (see Fig. 14) we see a different situation. Here, for small values of J_2/J χ_{CAF} is again dominant which is consistent with the proposed phase diagram. However, at a J_2/J value of approximately 0.35 χ_{CAF} dives down and χ_D soars. This would strongly seem to indicate a transition from a CAF phase to a dimer ordered phase. We also note that this occurs at

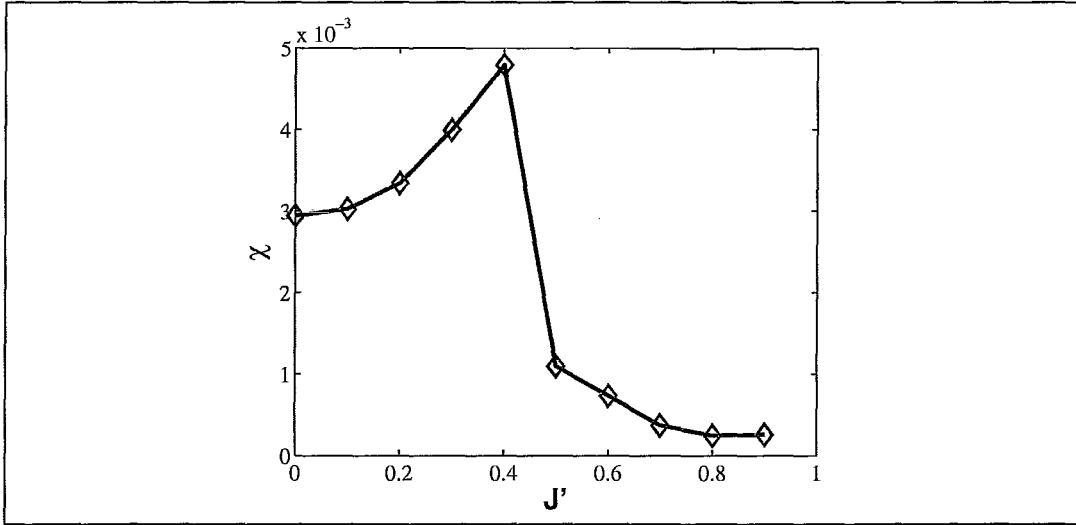


Fig. 13: For reference this diagram shows the results for the normal (non-CFFS) fidelity susceptibility. Notice the extremely low signal and ambiguous peak (whether it tends to infinity in the limit of infinite system size is unclear) and then sudden drop. This behaviour is difficult to interpret in terms of transitions between CAF, spiral and dimerized states.

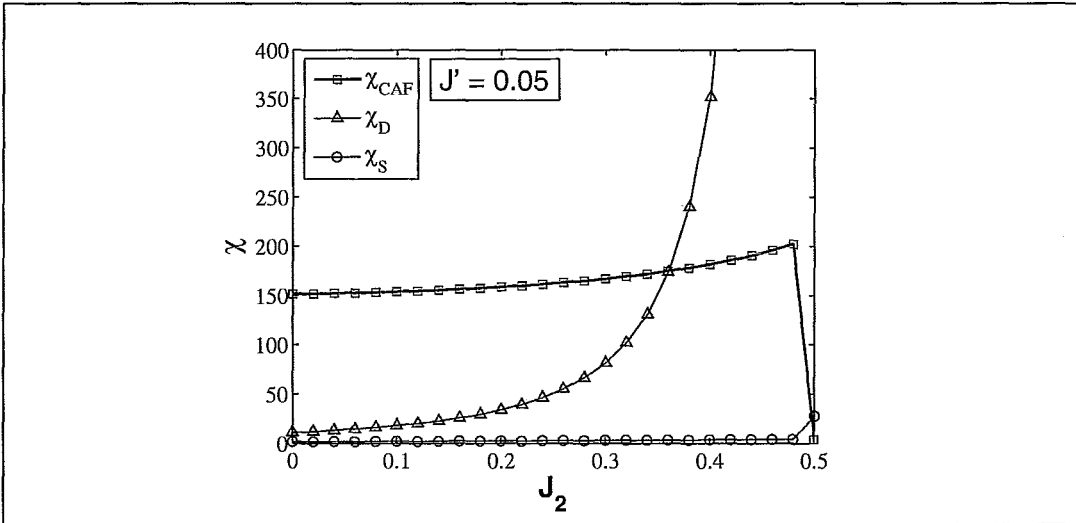


Fig. 14: This diagram shows a horizontal cross-section of the HATM phase diagram ($J' = 0.05$). Notice the initial domination of χ_{CAF} in the region $J' = 0.0 \dots 0.35$ at which point χ_{CAF} plummets and χ_D rises dramatically. We would take this as a strong indication of a transition from CAF ordering to dimer ordering.

~ 0.35 which is not close to the known value of 0.24 which must occur when $J' = 0$. This is evidence that one cannot make exact quantitative estimates of transition points using this method of competing magnitudes as is.

As a final attempt to flesh out the HATM phase diagram an analysis similar to that used for the spin-1/2 chain was performed. Intersection points of χ_D/L^3 were extrapolated using a power law fit to the limit of infinite system size. However, it is very important to note that for computational reasons calculations on increasingly large square lattices is not

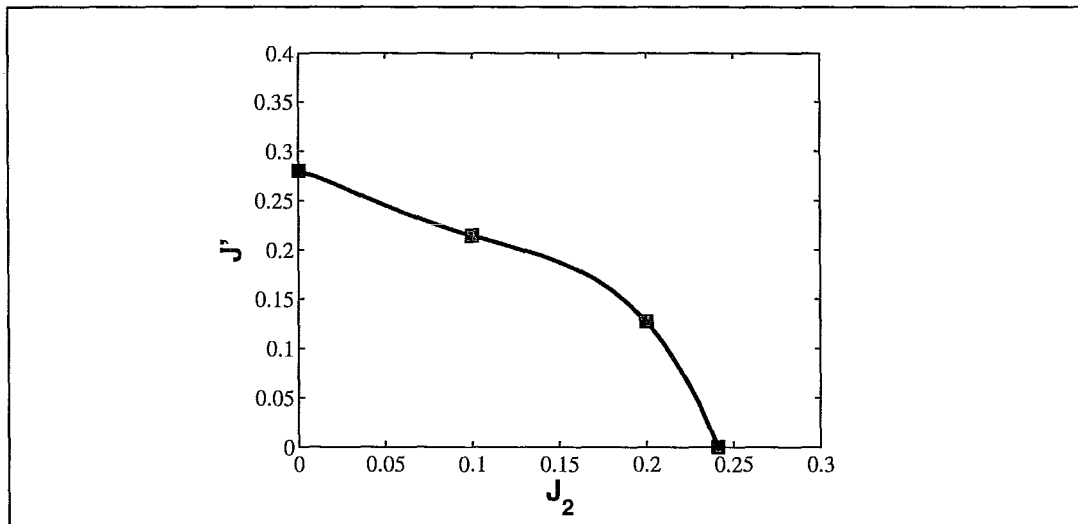


Fig. 15: This diagram shows the intersection points of χ_D/L^3 in the limit $L \rightarrow \infty$ for various values of J' and J_2 . Values were obtained by extrapolating power-law fits to infinity.

possible, they would quickly get far too large. Thus, these computations were performed on “triangular lattices” consisting of only *two* loosely coupled chains. To increase the system size the chains were then lengthened by a factor of 2 (meaning a total system size increase of 4) in order to produce the next smallest lattice capable of a correct dimer covering given periodic boundary conditions. This lack of two-dimensionality of the lattices will almost certainly have an effect on the results and thus they should be taken with a grain of salt. However, the results, which can be found in Fig. 15, indicate a possible issue. They would seem to suggest a transition to a dimerized state at $\sim J' = 0.28$ when moving vertically. This would seem to contradict the expectation of spiral ordering as J' is increased at constant J_2 . Nevertheless, these results may potentially be correct. By re-examining Fig. 12 we can see that χ_D rises with increasing J' before plateauing at $\sim J' = 0.7$ before dying out. If one were to attempt to provide separate weightings to each susceptibility in an attempt to make their magnitudes directly comparable then it is possible that χ_D may briefly overtake χ_{CAF} in the approximate region of $J' = 0.25 - 0.7$. If this is true then the system may transit first from a CAF state, then to a dimer state before finally entering a spiral state as J' is increased.

5.7 Discussion

The results of the relative magnitude CFFS method seem to bare out the HATM phase diagram proposed in the literature with the possible exception of a temporary transition to dimerized order before spiral ordering as one increases J' . We tentatively combine this information with additional cross-sections (see Fig. 16) to construct the phase diagram seen in Fig. 17a.

Clearly, this new method shows great promise as a means of establishing rough phase diagrams. If given a new substance with a theoretical model and one is unsure which of a number of ordered phases the substance is in then one can simply construct CFFS's for each phase and compare relative magnitudes. If one susceptibility is clearly dominant it is likely the substance is in that phase. Furthermore, one could implicitly identify spin-liquid phases by exhausting all possible ordered susceptibilities.

As to the effectiveness of this technique at identifying topological or higher-order tran-

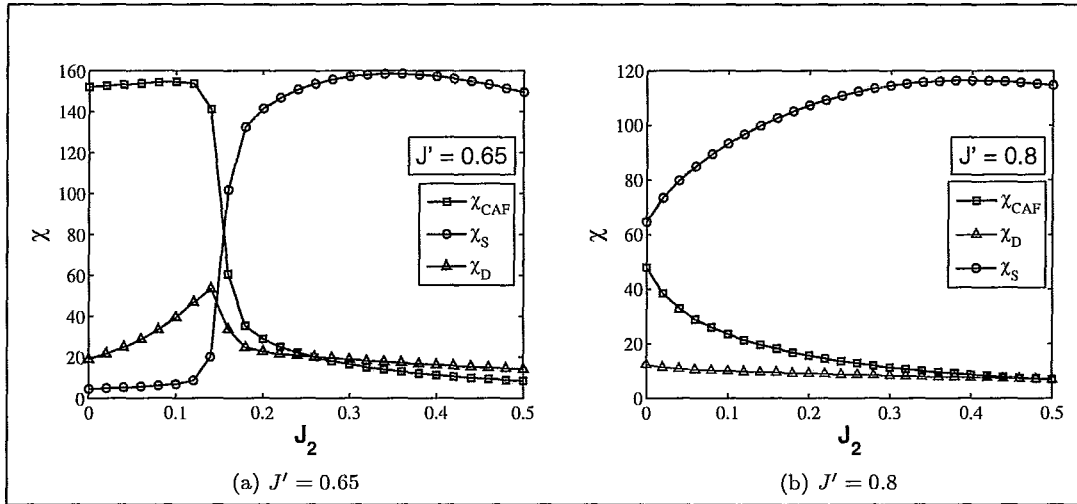


Fig. 16: These additional horizontal cross-sections are provided to show the behaviour of the phase diagram in the high J_2 , high J' region where it appears to be spiral ordered.

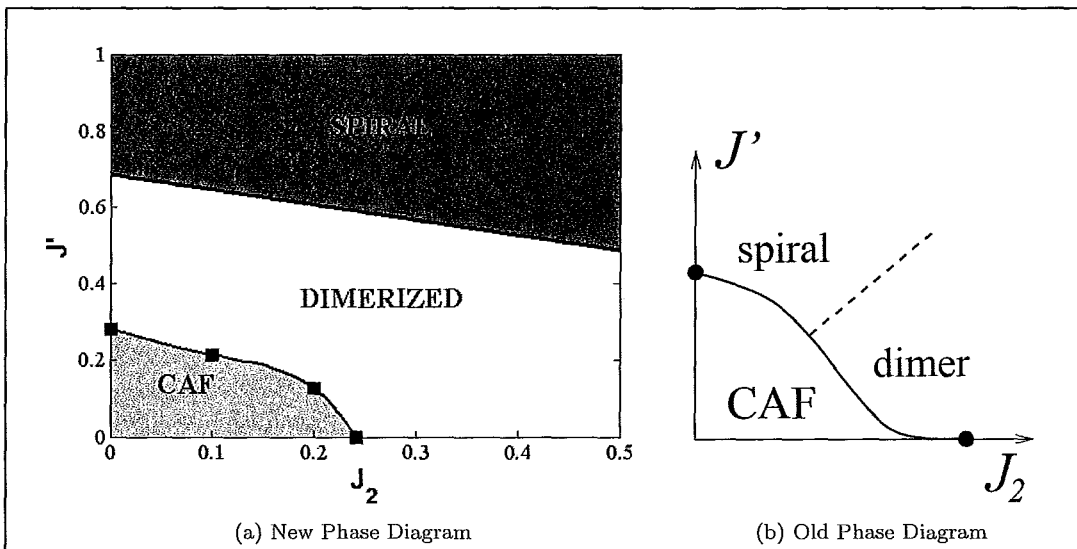


Fig. 17: Left: Our new proposed phase diagram which shows a region of dimerization before entering spiral ordering. Right: The old phase diagram suggested by Balents et al.[70]

sitions that still remains unclear. It has been shown to identify a BKT-type transition however, as was discussed previously, this may have been serendipity. Furthermore, the success of the CFFS method at identifying phases is contingent on the ability to describe a conjugate field and thus an order parameter for a system. However, it is a promising new method which may have great potential.

6 Conclusion and Summary

In this work we have briefly surveyed the history and construction of the fidelity and fidelity susceptibility as well as examined the numerical tools necessary to calculate quantum

ground-states. From there the Conjugate Field Fidelity Susceptibility (CFFS) was introduced as a new method of exploring quantum phase diagrams. It was first applied to the oft studied spin-1/2 chain where it successfully identified the $J_2 = 0.24$ transition point between the critical (Luttinger) phase and spontaneous dimerization. With some caveats this was taken as evidence that the CFFS technique could potentially be used to identify BKT-type transitions. The method was then applied to the Heisenberg Anisotropic Triangular Model (HATM) that has recently seen much interest due to its relation to Cs_2CuCl_4 , a material which is believed to exhibit a spin-liquid phase. Application of the CFFS method to the HATM confirmed the phase diagram proposed by the literature and possibly suggested a new region of dimerization living between collinear-antiferromagnetic (CAF) and spiral orderings. This evidences one of the advantages of the CFFS over other techniques in its ability to not only identify whether or not a transition occurs but between which two phases the system is transiting (by means of which susceptibilities are dominating). These results suggest that the CFFS method may be a useful new tool for exploring quantum phase transitions.

7 Future Work

The CFFS method is brand-new and has much room for improvement and modification. Of immediate interest is the ability to weight different susceptibilities such that their relative magnitudes can be directly compared. This would allow numerical estimates of transition points between phases. The CFFS should also be applied to more systems and phases so that its effectiveness at identifying higher-order and topological transitions can be gauged. Finally, there is a lot of interesting work that could be done at examining the theoretical under-pinnings of the CFFS itself. From this sort of study a better understanding of its regime of applicability could be obtained.

8 Bibliography

References

- [1] V. L. Beresinskii, Sov. Phys. JETP **32**, 493 (1971).
- [2] J. M. Kosterlitz and D. J. Thouless, J. Phys. C **6**, 1181 (1973).
- [3] C. C. Paige, J. Inst. Maths. Applics. **10**, 373-381 (1972).
- [4] C. C. Paige, J. Inst. Math. Phys. **18**, 341 (1976).
- [5] G. S. Tian and H. Q. Lin, Phys. Rev. B **67**, 245105 (2003).
- [6] H. Q. Lin, Phys. Rev. B **42**, 6561 (1990).
- [7] Jane K. Cullum and Ralph A. Willoughby, *Lanczos Algorithms for Large Symmetric Eigenvalue Computations Volume 1: Theory* (Birkhauser, Boston, 1985).
- [8] Alexander Weiß and Holger Fehske *Computational Many-Particle Physics*, Lect. Notes. Phys. 739, Chapter 18, (Springer, Berlin Heidelberg, 2008).
- [9] A. Uhlmann, Rep. Math. Phys. **9**, 273 (1976).

- [10] P. Alberti and A. Uhlmann, in *Proceedings of the Second International Conference on Operator Algebras, Ideals, and their Applications in Theoretical Physics*, edited by H. Baumgartel, G. Laner, A. Pietsch, and A. Uhlmann (1983).
- [11] P. M. Alberti, *Lett. Math. Phys.* **7**, 25 (1983).
- [12] P. M. Alberti and A. Uhlmann, *Lett. Math. Phys.* **7**, 107 (1983).
- [13] W. K. Wootters, *Phys. Rev. D* **23**, 357 (1981).
- [14] R. Jozsa, *J. Mod. Opt.* **41**, 2315 (1994).
- [15] B. Schumacher, *Phys. Rev. A* **51**, 2738 (1995).
- [16] C. A. Fuchs, *Distinguishability and Accessible Information in Quantum Theory*, Ph.D. Thesis, eprint, quant-ph/9601020.
- [17] A. Rastegin, *Sine distance for quantum states*, e-print, arXiv:quant-ph/0602112v1.
- [18] J. L. Chen, L. Fu, A. A. Ungar, and X. G. Zhao, *Phys. Rev. A* **65**, 054304 (2002).
- [19] Z. Ma, F. L. Zhang, and J. L. Chen, e-print, arXiv:0808.0984.
- [20] T. Gorin, T. Prosen, T. H. Seligman, and M. Znidaric, *Phys. Rep.*, **435**, 33-156 (2006).
- [21] P. E. M. F. Mendonca, R. d. J. Napolitano, M. A. Marchioli, C. J. Foster, Y. C. Liang, e-print, arXiv:0806.1150.
- [22] J. A. Miszczak, Z. Puchala, P. Horodecki, A. Uhlmann, and K. Zyczkowski, *Quantum Information & Computation* **9**, 103 (2009).
- [23] X. Wang, C. S. Yu, X. X. Yi, e-print, arXiv:0807.1781.
- [24] Shi-Jian Gu, arXiv:0811.3127
- [25] W. L. You, Y. W. Li, and S. J. Gu, *Phys. Rev. E* **76**, 022101 (2007).
- [26] Shu Chen, Li Wang, Shi-Jian Gu and Yupeng Wang, *Phys. Rev. E* **76**, 061108 (2007).
- [27] H. T. Quan, Z. Song, X. F. Liu, P. Zanardi, and C. P. Sun, *Phys. Rev. Lett.* **96**, 140604 (2006).
- [28] P. Zanardi and N. Paunkovic, *Phys. Rev. E* **74**, 031123 (2006).
- [29] P. Zanardi, M. Cozzini, and P. Giorda, *J. Stat. Mech.* **2**, L02002 (2007).
- [30] M. Cozzini, P. Giorda, and P. Zanardi, *Phys. Rev. B*, **75**, 014439 (2007).
- [31] M. Cozzini, R. Ionicioiu, and P. Zanardi, *Phys. Rev. B*, **76**, 104420 (2007).
- [32] P. Buonsante and A. Vezzani, *Phys. Rev. Lett.* **98**, 110601 (2007).
- [33] P. Zanardi, P. Giorda, and M. Cozzini, *Phys. Rev. Lett.* **99**, 100603 (2007).
- [34] H. Q. Zhou, e-print, arXiv:0704.2945.
- [35] H. Q. Zhou, J. H. Zhao, and B. Li, *J. Phys. A: Math. Theor.* **41**, 492002(2008).
- [36] H. Q. Zhou, J. H. Zhao, H. L. Wang, and B. Li, e-print arXiv: 0711.4651.
- [37] Shu Chen, Li Wang, Yajiang Hao, and Yupeng Wang, *Phys. Rev. A* **77**, 032111 (2008).

- [38] M. F. Yang, Phys. Rev. B **76**, 180403 (2007).
- [39] L. C. Venuti, M. Cozzini, P. Buonsante, F. Massel, N. Bray-Ali, and P. Zanardi, Phys. Rev. B **78**, 115410 (2008).
- [40] S. Yang, S. J. Gu, C. P. Sun, and H. Q. Lin, Phys. Rev. A **78**, 012304 (2008).
- [41] D. F. Abasto, A. Hamma, and P. Zanardi, Phys. Rev. A **78**, 010301 (2008).
- [42] H. A. Bethe, Z. Phys. **56**, 205 (1931).
- [43] R. J. Baxter, *Exactly solved models in statistical mechanics*, (London, Academic Press, 1982)
- [44] C. K. Majumdar and D. K. Ghosh, J. Math. Phys. **56**, 1388 (1969); 10, 1399 (1969).
- [45] F. D. M. Haldane, Phys. Rev. B **56**, 4925 (1982).
- [46] T. Giamarchi, *Quantum Physics in One Dimension* (Oxford University Press, Oxford, England, 2004).
- [47] T. Tonegawa and I. Harada, J. Phys. Soc. Jpn. **56**, 2153 (1987).
- [48] S. Eggert, Phys. Rev. B **54**, R9612 (1996).
- [49] R. J. Bursill et al., J. Phys. C **7**, 8605 (1995).
- [50] R. Chitra, S. Pati, H. R. Krishnamurthy, D. Sen, and S. Ramasesha, Phys. Rev. B **52**, 6581 (1995).
- [51] S. R. White and I. Affleck, Phys. Rev. B **54**, 9862 (1996).
- [52] K. Okamoto and K. Nomura, Phys. Lett. A **169**, 433 (1992).
- [53] G. Castilla, S. Chakravarty, and V. J. Emery, Phys. Rev. Lett. **75**, 1823 (1995).
- [54] I. Affleck, D. Gepner, H. J. Schulz, and T. Ziman, J. Phys. A **22**, 511 (1989).
- [55] John W. Negele, Henri Orland *Quantum Many-Particle Systems*, (Westview Press, 1988).
- [56] L. E. Reichl, *A Modern Course in Statistical Physics*, (John Wiley & Sons, Inc., 1998)
- [57] K. Huang, *Statistical Mechanics*, (John Wiley & Sons, Inc., 1963)
- [58] L. C. Venuti and P. Zanardi, Phys. Rev. Lett. **99**, 095701 (2007).
- [59] S. J. Gu, H. M. Kwok, W. Q. Ning, and H. Q. Lin, Phys. Rev. B **77**, 245109 (2008).
- [60] H. M. Kwok, W. Q. Ning, S. J. Gu, and H. Q. Lin, e-print, arXiv:0710.2581.
- [61] R. Coldea, D. A. Tennant, and Z. Tylczynski, Phys. Rev. B **68**, 134424 (2003).
- [62] P. W. Anderson, G. Baskaran, Z. Zou, and T. Hsu, Phys. Rev. Lett. **58**, 2790 (1987).
- [63] C.H. Chung, K. Voelker, and Y.B. Kim, Phys. Rev. B **68**, 094412 (2003).
- [64] S.V. Isakov, T. Senthil, and Y.B. Kim, Phys. Rev. B **72**, 174417 (2005).
- [65] J. Alicea, O.I. Motrunich, and M.P.A. Fisher, Phys. Rev. Lett. **95**, 247203 (2005).

- [66] R. Coldea et al., Phys. Rev. Lett. **86**, 1335 (2001).
- [67] M.Y. Veillette, J.T. Chalker, and R. Coldea, Phys. Rev. B **71**, 214426 (2005).
- [68] M.Y. Veillette, A.J.A. James, and F.H.L. Essler, Phys. Rev. B **72**, 134429(2005).
- [69] D. Dalidovich et al., Phys. Rev. B **73**, 184403 (2006).
- [70] O.A. Starykh and L. Balents, e-print, arXiv:cond-mat/0607386v2
- [71] O.A. Starykh and L. Balents, Phys. Rev. Lett. **93**, 127202 (2004).
- [72] O.A. Starykh, A. Furusaki, and L. Balents, Phys. Rev. B **72**, 094416 (2005)
- [73] M. Q. Weng, D. N. Sheng, Z. Y. Weng, and Robert J. Bursill, Phys. Rev. B **74**, 012407 (2006).
- [74] S. Yunoki and S. Sorella, Phys. Rev. B **74**, 014408 (2006).
- [75] D.Heidarian, S. Sorella, and F. Becca, Phys. Rev. B **80**, 012404 (2009).
- [76] O. A. Starykh and L. Balents, Phys. Rev. Lett. **98**, 077205 (2007).
- [77] R. F. Bishop, P. H. Y. Li, D. J. J. Farnell, and C. E. Campbell, Phys. Rev. B **79**, 174405 (2009).
- [78] O. A. Starykh, H. Katsura, and L. Balents, Phys. Rev. B **82**, 014221 (2010).
- [79] W. Zheng, R.H. McKenzie, and R.R.P. Singh, Phys. Rev. B **59**, 14367 (1999).
- [80] A.A. Nersesyan, A.O. Gogolin, and F.H.L. Essler, Phys. Rev. Lett. **81**, 910 (1998). B **72**, 094416 (2005).